Effects of Soil Arching on Behavior of Pile-supported Railway Embankment: 2D FEM approach

Naveen Kumar Meena[1], Sanjay Nimbalkar[2#], Behzad Fatahi[3], Gui Yang[4]

[1]Ph.D. candidate, School of Civil and Environmental Engineering, University of Technology Sydney, Ultimo NSW 2007, Australia. E-mail: Naveenkumar.Meena@student.uts.edu.au

https://orcid.org/0000-0001-9678-0950

[2#]Senior Lecturer, School of Civil and Environmental Engineering, University of Technology Sydney, Ultimo NSW 2007, Australia. E-mail: Sanjay.Nimbalkar@uts.edu.au (Corresponding Author)

ORCID ID: https://orcid.org/0000-0002-1538-3396

[3]Associate Professor, School of Civil and Environmental Engineering, University of Technology Sydney, Ultimo NSW 2007, Australia. E-mail: Behzad.Fatahi@uts.edu.au

ORCID ID: https://orcid.org/0000-0002-7920-6946

[4]Associate Professor, School of Civil and Transportation, Hohai University, Xikang Road, Nanjing, Jiangsu, China Post Code: 210098. E-mail: ygheitu@163.com

Submitted to: Computers and Geotechnics, Elsevier

Number of Pages = 28, Tables = 5, Figures = 15

Author for correspondence:

Dr. Sanjay Nimbalkar
Senior Lecturer, School of Civil & Environmental Engineering
Centre for Built Infrastructure Research (CBIR)
Faculty of Engineering & Information Technology
University of Technology Sydney
CB11.11.221, City Campus, 15 Broadway, Ultimo NSW 2007 Australia
Tel: +61 2 9514 1819
Email: Sanjay.Nimbalkar@uts.edu.au

Effects of Soil Arching on Behavior of Pile-supported Railway Embankment: 2D FEM approach

Naveen Kumar Meena[1], Sanjay Nimbalkar[2#], Behzad Fatahi[3], Gui Yang[4]

ABSTRACT

The construction of railway embankment on soft soil is a challenging task for practitioners. In the past, several approaches have been employed in practice to overcome this problem. Pile foundation is considered one of the reliable solutions for soft ground. In a pile-supported railway embankment, soil arching plays a vital role in the efficient load transfer to the piles. In this study, the soil arching phenomenon in a granular embankment subjected to train induced loading is demonstrated based on the two-dimensional (2D) finite element modeling approach. A 2D plane strain idealization is used to convert a real three-dimensional (3D) case into 2D. The effects of the piled railway embankment properties on soil arching are investigated. It is found that pile modulus, embankment modulus and friction angle affect the arching mechanism significantly. Pile spacing (*s*) variation affects soil arching (i.e., the arching zone can be increased by reducing s). In addition, the height and shape of arching are studied. A comparison with the available analytical design methods for embankments is presented which indicates inconsistencies in the previously published results.

Keywords: Railway, Piled-embankment; finite element modeling; soil arching.

1. Introduction

The population growth in Australia is responsible for significantly increased construction activities over unsuitable lands, such as coastal and low-lying marshy areas characterised by thick deposits of soft compressible soil. The sustainable performance of transport infrastructures on such soils requires innovative construction and ground improvement techniques. Embankments are widely used to elevate the ground level for the construction of railways on soft soils. However, soft soils pose problems of low bearing capacity, large deformations and lateral movement, resulting in a longer construction time or preconstruction failure.

In the past, several approaches have been used to address these challenges, such as: (i) preloading or staged construction [1], (ii) insertion of vertical drains [2], (iii) use of the lightweight embankment fill materials [3], (iv) height reduction or slope flattening of the embankment, and (v) the addition of column supports [4]. The column supports can be rigid such as piles [5], semi-rigid like cement mix columns [4, 6] or flexible as stone columns [7]. The benefits associated with the use of pile supports are: (i) stiffening of the surrounding subsoil which, in turn, prevents the horizontal movement of subsoil; (ii) reducing embankment settlement and allowing construction to occur in a single stage without any construction delays or preconstruction failure; and (iii) suitability for complex geological conditions and adjacent to service utilities, such as cables and pipelines [8].

In a piled embankment, embankment fill tends to settle more in the regions between columns due to stiffness differences between piles and the surrounding soil. However, this downward movement is restricted by mobilized shear resistance. Due to this shear resistance, the stress exerted on the soft ground is reduced while transferring to the piles. This load transfer mechanism, known as soil arching, as introduced by Terzaghi [9].

The soil arching mechanism has been described by soil arching ratio (*SAR*) and efficacy (E_{str}). The soil arching ratio (*SAR*) is defined as [10]:

$$SAR = \frac{\sigma_s}{(\gamma h + q)} \quad (1)$$

where, σ_s is subsoil stress; γ is the unit weight of embankment fill; h is embankment height, and q is the applied surcharge over the embankment. *SAR* is also known as the stress reduction ratio in the literature. *SAR* lies between 0 and 1. *SAR* = 0 represents the formation of full soil arching, i.e. entire embankment load is transferred to the piles. In contrast, *SAR* = 1 denotes no soil arching, implying the stress applied to the subsoil is equal to the embankment load [7, 11].

The efficacy (E_{str}) measures the portion of the embankment load transferred to the piles and is expressed as [12]:

$$E_{\mathrm{str}} = \frac{Q}{s^2 \gamma h} \quad (2)$$

where, Q is the total force carried by the pile; γ is the unit weight of the embankment fill; h is the embankment height; s is the pile spacing.

In the past, various numerical [8, 13-16] as well as experimental studies [14-17] were carried out to investigate the load transfer mechanism in a piled embankment. A numerical study performed by Han and Gabr [8] considered the impact of three factors namely: embankment height, tensile stiffness of geosynthetics, and the elastic modulus of the pile on the load transfer mechanism. Jenck et al. [13] showed an increase in efficacy with the increase in embankment height. They assumed static load to represent traffic scenario and neglect the dynamic effect of traffic speed and associated loading. Ariyarathne et al. [14] analyzed an actual piled embankment in both three-dimensional (3D) and two-dimensional (2D) condition. Different idealization methods were used in 2D plane-strain condition and found that equivalent area

(EA) method yielded the closest results to 3D and field results. Bhasi and Rajagopal [15] studied the influence of embankment fill properties, and the pile modulus considering 2D axisymmetric and 3D models. They also reported that the efficacy is affected by friction angle. Most of these studies assumed that soil arching is the principal mechanism for load transfer to the pile, and considered the arrangement of piles in a square pattern. Nunez et al. [18] concluded that consider all the design methods overestimated stress efficacy; while settlement efficacy was a reliable parameter to assess the overall performance of the piled embankment. Settlement efficacy (E_{set}) is termed as [18].

$$E_{\text{set}} = 1 - \frac{\delta_p}{\delta} \tag{3}$$

where, δ_{p} and δ are the soil settlements with and without piles, respectively.

In summary, the past studies were primarily concerned either on; 1) influence of piled embankment parameters on the load transfer mechanism; or 2) height of soil arching, considered static load as traffic scenario with the piles arrangement in a square pattern.

The pile-supported embankments are increasingly being used to support the railway tracks in areas where soft ground is encountered. Numerous numerical studies have investigated the soil arching mechanism in a pile-supported railway embankment [8, 13]. However, these studies considered static loading and neglected the effect of train speed and associated loading. It is widely acknowledged that the increase in train speed would impose higher stresses on track foundations [21-22]. In addition, the past studies have considered the arrangement of piles in a square pattern [8, 13, 15]. However, a triangular pattern can be useful for railway embankments [23]. Therefore, this study addresses the effects of train loading and pile arrangement on the stability of pile-supported railway embankment.

In view of these, the finite element (FE) method is used to provide an insight into the behavior of the railway embankment supported by piles that are arranged in a triangular pattern with particular emphasis on the soil arching mechanism. The present study is focused on the parameters as mentioned earlier to identify their influence on the size and shape of soil arching and find the most critical parameters with optimum value for effective load transfer against the train induced loading. The comparison of different analytical methods has also been reported to identify the variation and selection of an appropriate method.

The present study comprises of (i) calibration of the numerical model with existing experimental data, (ii) Comparison of the soil arching mobilization in embankment supported by piles that are arranged in two different patterns (i.e., square and triangular), (iii) comprehensive study focusing on the size and shape of soil arching to investigate the most critical parameters, and (iv) a comparison with the available design methods.

1.1 Two-dimensional (2D) idealization

Typically, pile-supported railway embankment is a 3D problem. However, 3D modeling is complex, time-consuming and needs advanced computing facility. Therefore, 2D plane strain modeling is used with reasonable accuracy in practice to overcome these problems [14, 24].

Various approaches such as equivalent area (EA), area replacement ratio (ARR), equivalent flexural stiffness (EFS) and equivalent elastic modulus (EEM) of piles are used to transform a 3D problem to 2D. The highlighted region of a piled embankment, as shown in Figure 1(a) is adopted for 2D approximation. The soil arching is investigated in terms of vertical stress, settlement and lateral stress coefficient above the center of the subsoil (point A) and piles (point B), as shown in Figure 1(b).

In the EA method, the individual piles and surrounding soil are considered as a composite area. Individual piles are converted into plane strain wall with an equivalent thickness (d), calculated by Eq. (4). The material properties for a converted wall are considered the same as used in 3D for individual piles.

$$d = \frac{\pi D^2}{4s} \tag{4}$$

where, D is the diameter of the circular pile, and s is center to center pile spacing between two piles, which is arranged in a square pattern.

2. Numerical Modeling

2.1 Description and Material properties

The finite element method (FEM) based software, ABAQUS - version 2013 [25] is used to simulate a piled railway embankment model in a plane strain (2D) condition. Figure 1(b) represents a typical mesh profile of a piled-embankment model (h = 3.5 m and s = 2.5 m). The vertical sides represent the lines which pass through the center to center pile spacing (s) and above the embankment fill, including the gravel bed. The 1383 eight-node, reduced-integration, two-dimensional, quadratic (second-order) solid elements (CPE8R) are used in this analysis. The reduced integration uses a lesser number of Gaussian co-ordinates when solving the integral and reduces computational time. Further, second-order reduced-integration elements provide more accurate results than the corresponding integrated elements.

A unit cell model with center to center pile spacing (s) is used for this study (refer Figure 1a). Roller supports were used on the vertical boundaries, restricting horizontal movement. The fixed support condition is used for the horizontal bottom boundary to completely restrict displacement. No boundary conditions are considered at the top of the embankment. The

bottom boundary represents the base of the piles and subsoil, which is underlain by half-pile wall (width, $d/2$) on both sides and subsoil [width, (s-d)] at the middle of the piles. The pile diameter (D) is fixed at 1.0 m, and the center to center pile spacing (s) is 2.0, 2.5 or 3.5 m (e.i., pile width (d) is changing according to the pile spacing). The embankment height (h) varies from 2.5 to 6.5 m, including a 400 mm thick gravel bed at the embankment bottom. The depth of the subsoil and length of the pile are the same, both being 8 m.

2.1.1 Material properties

The embankment fill, gravel bed and subsoil are considered as sand fill, well-graded gravel, and silty sand, respectively. A linear elastic-perfectly plastic model with Mohr-Coulomb failure criterion is used for the embankment fill and subsoil material. In the research studies available in literature, the performance of embankments and subsoil were successfully simulated by the linear elastic-perfectly plastic model with Mohr-Coulomb failure criterion, and reasonable predictions of soil arching were obtained [24, 26-27]. The unsaturated soil and the corresponding constitutive model was not considered. The soil was assumed to remain in the dry state with facilitation of the fully drained conditions owing to the coarse-grained nature of materials used as the embankment fill and gravel bed. All the parameters used in the analyses are summarized in Table 1.

2.1.2 Interface

In this study, basic Coulomb friction model was used to simulate the interaction of pile with the surrounding soil. This model allows the contacting surfaces (i.e., the surface of pile and subsoil) to carry shear stresses before sliding. The surface to surface contact is provided between pile and surrounding soil. The normal contact is considered as “hard contact” as it is able to transfer normal stress under compression, while under tension pile and soil will

separate. The tangential contact is provided as penalty contact with a frictional coefficient at interface between the pile and surrounding soil. The interface frictional coefficient is given by:

$$\mu = \tan\delta \tag{5}$$

where, δ is the interface friction angle between pile and the surrounding subsoil, and it can be determined as [28-30]:

$$\tan\delta = (0.5 - 1.0)\tan\phi' \tag{6}$$

where, ϕ' is the friction angle of the soil. In this study, the ratio of the interface friction coefficient ($\tan\delta$) and the soil friction coefficient ($\tan\phi'$) is assumed to be 0.7 for pile - subsoil interface.

2.2 Model calibration

The model calibration was performed against the experimental result (settlement above and amid the pile) for pile arrangements in a square pattern with dense sand sample reported by King et al. [31] to ensure the accuracy of the numerical modelling (refer Figure 2). Material properties of the embankment are taken as reported by King et al. [31], whereas appropriate properties of subsoil have been assumed. King et al. [31] obtained the settlement results for the different increment of normalized settlement plate displacement (δ_{sp}/b'). However, in this study only δ_{sp}/b' =2.8-4.0 % has been considered for validation. Four different idealization methods as discussed in the earlier section are used to convert 3D into 2D plane strain. It is found that the EA method shows an acceptable agreement between numerical modeling and experimental result, which serves the basis of further analysis for this study.

2.3 Stress determination on the pile-supported embankment

A typical railway track is considered above the pile-supported embankment (refer Figure 1a). In this study, the true dynamic nature of traffic loading and the dynamic response of the soil is not considered. The applied vertical load is equivalent dynamic load. The magnitude of the equivalent dynamic load is equal to the weight of the train multiplied by an impact factor (i.e., dynamic amplification factor), which accounts for the dynamic effects due to the moving train as [22, 32-33]:

$$F_{\mathrm{d}} = \Phi\, F_{\mathrm{s}} \tag{7}$$

where, F_d is design wheel load (kN) incorporating dynamic effect, F_s is static wheel load (kN), and Φ is dimensionless dynamic impact factor. Various empirical methods such as Eisenmann, American Railways Engineering Association (AREA), and Office of Research and Experiments (ORE) are widely used to calculate dynamic amplification factor (DAF) catering for the effect of train speed. In this study, ORE method is adopted to determine dynamic impact factor as this method is most relevant to Australian conditions. In this method, the DAF is defined in terms of dimensionless speed coefficients as given by following equation:

$$\Phi = 1 + \alpha' + \beta' + \gamma' \tag{8}$$

where, $\alpha'$and β' are associated with mean value of impact factor, and γ' is related to the standard deviation of the impact factor. Details on the calculations of DAF using various methods are provided in Table 2.

Various alternatives such as Odemark, Zimmermann, Trapezoidal approximation (2:1), and AREMA exist to calculate the maximum vertical stress on a subgrade [32]. In this study, the maximum vertical stress is calculated by Trapezoidal approximation (2:1) method due to their simplicity. A train speed varying from 40 to 160 km/h is considered. Train-induced vertical stresses (σ_{t}) corresponding to 40-160 km/h speeds are determined as 105-118 kPa which is

227 applied the top of the modeled unit cell. More details on train-induced vertical stresses are
228 provided in Table 3.

229 ### *2.4 Effect of pile arrangement on soil arching*

230 Figure 3 demonstrates the effect of pile arrangement on the degree of soil arching. The pile
231 arrangement is considered in a square and triangular pattern. Influence of an individual pile is
232 assumed square and hexagonal soil block, when pile arranged in a square and triangular pattern,
233 respectively. As earlier discussed that EA method serves the basis of further analysis, the
234 square block (i.e., piles arranged in a square pattern) is easy to convert into plane strain wall
235 using Eq (4). However, the hexagonal block (i.e., pile arranged in a triangular pattern) first
236 converted into a square-shaped block of equivalent area. The width of the equivalent square
237 block is considered as the pile spacing (s) and converted into plane strain wall. It is evident that
238 pile arranged in a triangular pattern can demonstrate more efficient load transfer mechanism
239 compared to square pattern. Therefore, the pile arrangement in triangular pattern is used for
240 further analysis.

241 ## 3. Results and discussion

242 ### *3.1 Vertical stress*

243 The vertical stress profile in the railway embankment fill (including the gravel layer) can be
244 used to assess the soil arching phenomenon. Figure 4 shows the vertical stress contours for
245 different embankment heights and pile spacing above point A and point B. The vertical stress
246 (σ) is normalized by $\gamma(s\text{-}d)$, whereas the varying embankment height (h) is normalized by (s-
247 d). Figure 4(a) shows the vertical stress contours for three embankment height (i.e., 2.5 m, 3.5
248 m, and 5.0 m) fixed at pile spacing (s) 2.5 m. It is observed that the variation of vertical stress
249 along the normalized embankment height increases on the point B for all considered

250 embankment height and demonstrate the soil arching phenomena. For a specified embankment
251 height (h), the vertical stress initially increases with a gradient equal to overburden stress
252 extending from the embankment-fill top to the outer boundary of the soil arch. The stress profile
253 then disturbed (decreases on point A and increase on point B). At this level, the majority of the
254 embankment load is transferred onto the pile. It is worth mentioning that in this study the full
255 soil arching developed with 1.3(s-d) (outer boundary) and 0.25(s-d) (inner boundary) after h =
256 5 m, which is quite similar to the studies in the past (refer Table 4).

257 Figure 4(b) shows the vertical stress contours for a fixed embankment height (h = 3.5 m) varied
258 with three pile spacing (s) (i.e., 2.0 m, 2.5 m, and 3.5 m). For s = 2 m, the arching height
259 increases more compared to s = 2.5 m and 3.5 m, whereas the inner boundary remains the same
260 (i.e., independent of spacing variation). It shows that pile spacing (s) variation affects soil
261 arching (i.e., the arching zone can be increased by reducing s). The arching zone is referred to
262 as the thickness of the soil arch. Due to the expansion of this zone, more load is transferred to
263 the pile.

264 *3.2 Comparison with Hewlett and Randolph* [12] *predictive method*

265 Fagundes et al. [19] and Zhuang et al. [34] proposed three failure modes at the maximum
266 arching to compare the observed behavior with the Hewlett and Randolph method [12]. Figure
267 5 shows the ultimate subsoil stress (σ_s), illustrating the variation in normalized embankment
268 height (h/s). The ultimate subsoil stress is normalized by γs. These three failure mechanisms
269 (i.e., no arching, failure at the crown, and failure at pile head) are shown in Figure 5 by dotted
270 (for no arching, and failure at pile head) and solid lines (failure at the crown). The different
271 colored solid lines show the FE results for different s.

The first mechanism is stipulated for the 'no arching' condition (i.e., $\sigma_s = \gamma h$). In the second mechanism, the failure is based on the limiting conditions at the crown of the soil arch (failure at the crown). This mechanism indicates $\sigma_s = 0.5\gamma s$ which corresponds to the nominal weight beneath the crown of the hemisphere. The third mechanism is related to failure at the pile head or punching the pile head into the base of the embankment. Additional, failure at the crown of the arch in the plane strain condition, as proposed by Low et al. [10] is shown by the dotted centerline. The results plotted in Figure 5 show similar trends with other studies [19, 34].

It is evident that the stress value on the subsoil is less than $0.5\gamma s$ (approximately representing the weight of the material below the top of the semicircular arch) up to a critical value of (h/s). At a higher (h/s) value, conditions at the pile head are more critical as also reported by Hewlett and Randolph [12]. However, for plane strain conditions, Hewlett and Randolph [12] predict that conditions at the crown of the arch are always critical. Figure 5 demonstrates the FE results for failure occurring at the pile cap in terms of a simplified plane strain equation and resembling a three-dimensional failure state for the pile cap, as proposed by Hewlett and Randolph [12]. At the higher embankment height, it shows quite a similar trend of failure. However, the values from the plane strain failure appear to be overestimated for all pile spacing, especially as pile spacing (s) reduces.

3.3 Settlement

The settlement of railway embankment, especially when located on soft soils, is the crucial factor governing the embankment design and construction stages. Soil arching minimizes the settlement of the subsoil by load transfer onto the piles.

Figures 6 shows the normalized settlement contours for the embankment on the vertical side through point A and point B (refer Figure 1b). Figures 6(a) and 6(b) show the settlement

295 contour for varied h and s, respectively. The embankment height (h) and settlement were
296 normalized by the clear spacing between the adjacent pile head (s-d).

297 The differential settlement of the fill material above the pile head generates shear stresses that
298 extend upward into the fill material. When the embankment is sufficiently high, it is assumed
299 that the shearing force terminates at some horizontal plane: this plane is termed the plane of
300 equal settlement. Above this plane, no differential settlement occurs, indicating that the vertical
301 stress above this plane is not disturbed. However, below this plane, the embankment settlement
302 over point A increases to a maximum value, while it reduces to almost zero over point B. It
303 implies that the soil arching exists below the plane of equal settlement due to the differential
304 settlement of the embankment fill over point A and point B.

305 As shown in Figure 6(a), after a certain embankment height (5 m for this study) there is no
306 differential settlement (i.e., the existence of plane of equal settlement). It is observed that the
307 plane of equal settlement is located at the normalized embankment height of 1.75 (i.e., h = 3.78
308 m) and soil arching develops under this height. It is worth noting that the settlement on point
309 A increases with an increase in h.

310 In addition, Figure 6(b) shows that the settlement contour for different pile spacing. It is
311 observed that settlement increases with an increase in s. For s = 2 and 2.5 m, the plane of equal
312 settlement occurs corresponding to the normalized height of 1.34 and 1.6, respectively.
313 However, no plane exists for s = 3.5 m owing to the non-formation of soil arching.

314 ### *3.4 Settlement ratio (δ_{em}/δ_p)*

315 The differential settlement at the embankment top is defined as the difference between the
316 maximum settlement at the top surface of the embankment above point A and B (refer Figure
317 1) (i.e., δ_{em}-δ_p). However, the settlement ratio (δ_{em}/δ_p) can be employed to represent the

differential settlement. As evident, the settlement ratio (δ_{em}/δ_p) at the surface of the embankment is practically significant, in view of the embankment stability.

Figure 7(a) shows the settlement ratio variation with normalized embankment height (h/s). For (h/s) > 1.7, δ_{em}/δ_p becomes one, implying uniform settlement. As h decreases, δ_{em}/δ_p increases, while showing a steep increase for (h/s) < 1. Figure 7(b) demonstrates the increase in settlement ratio at point A (δ_{em}/δ_s), with an increase in h/s for the entire range of pile spacing (s) considered in this study. For s = 3.5 m and low embankment height ($h \leq 3.5$ m), δ_{em}/δ_s decreases as the soil arching is not fully developed. However, for higher embankment (h > 3.5 m), soil arching is fully developed as indicated by the increase in δ_{em}/δ_s.

3.5 Lateral stress coefficient (K)

The lateral stress coefficient (K) [Eq. (9)] is plotted on a vertical profile at point A and point B, further demonstrating soil arching. Figure 8 shows the lateral stress coefficient (K) profiles for a range of h and s, plotted with vertical distance upwards from the base of the embankment (h) normalized by (s-d). The results do not extend to the top of the embankment for higher embankments. Only the values of 0.25(s-d), 0.5s and 1.5(s-d) are highlighted on the Y-axis; and $K = K_a$ (= 0.33); K_0 (= 0.5) and K_p (= 3.0, considering the standard Rankine passive value and ignoring the small value of cohesion) on the X-axis. Figures 8(a) and 8(b) represent the K profile for varied h and s = 2.5 m at point A and point B respectively, whereas Figures 8(c) and 8(d) show the equivalent plot for h = 3.5 m at different s.

$$K = \frac{\sigma_h'}{\sigma_v'} \tag{9}$$

Referring to Figure 8(a) for [h/(s-d)] > 1.5, K is deduced to K_0 and is not influenced by soil arching. For the embankment height (h) > 2.5, K increases with depth for h/(s-d) < 1.5, approaching K_p when h = 0.25(s-d). Although for h =2.5, K tends to approach the K_0 stage;

however, the complete K_0 stage is not achieved due to lower h (undeveloped soil arching). The lower embankments (i.e., $h < 2.4$) show that stress along the entire height of the embankment is under the passive state. Figure 8(b) shows K profile at point B, an active state observed for higher embankments when $h/(s\text{-}d) < 1.0$, and K returns to K_0 at a similar height to Figure 8(a) which implies that for embankment (h) > 3.5, no stress disturbance occurred.

As discussed earlier, Figure 8(c) shows K profile at point A for $h = 3.5$ m at different s, resulting in the outer boundary of arch being dependent on s. The inner boundary remains the same for different s, also referred to in Figure 4(b). Moreover, Figure 8(d) shows the equivalent plot at point B for different s. The K profile returns to at rest (K_0) after the active state for $s = 2$ m, and 2.5 m. Further increments in s will not result in the K value returning to K_0 owing to the non-formation of soil arching.

The results observed in Figure 8 are consistent with the three-dimensional arch theory proposed by Hewlett and Randolph [12] in that the terms of active and passive conditions are perceived above point B and at the crown of the arch (at least near the inner boundary), respectively. These conditions are associated with the punching of the pile into the base of the embankment (for the active condition) and failure of the arch at the mid-span (for the passive condition), respectively. It may be observed that the effect on the stress state throughout the embankment fill is more widespread (higher) than the proposed discrete hemispherical boundaries since there is a gradual (rather than instantaneous) transition to K_0 as h increases.

4. Parametric study

A parametric study is incorporated to see the effect of different material parameters on the size and shape of soil arching. Once the basic plane strain model is verified by the results available from past studies, the analysis is further extended for the effect of a range of input parameters on soil arching. It will help to understand the effect of different input parameters on soil

365 arching. Only one parameter is changed at a time, while the others are kept at standard case
366 values. The details of these parameters were given in Table 1.

367 ### *4.1 Settlement ratio (δ_{em}/δ_p)*

368 For settlement ratio, embankment height is taken as 3.5 m (h is fixed) whereas pile spacing is
369 varied (s = 2.0, 2.5 and 3.0 m). The effect of pile modulus (E_p) and embankment modulus (E_{em})
370 on the ratio (δ_{em}/δ_p) for pile spacing 2.5 m is demonstrated in Figure 9(a). It shows a trend
371 which is depending on the E_{em} value (i.e., the settlement ratio increases 2 % with an increase
372 in E_p when the E_{em} has a minimum value, while the settlement ratio decrease by 3 % with an
373 increase in E_p when the E_{em} has maximum value). It implies that the pile modulus (E_p) should
374 be enough with maximum embankment modulus (E_{em}) to reduce the differential settlement at
375 embankment surface. A similar trend has been found for s = 2 and 3.5 m. Figure 8(b) indicates
376 the effect of friction angle (ϕ) and dilation angle (ψ) for s = 2.5 m. It can be seen that the
377 settlement ratio increases by 17 % with an increase in friction angle. The dilation angle does
378 not affect much δ_{em}/δ_p. However, for higher friction angle with lower dilation angle shows a
379 higher value of the settlement ratio. An increase in pile spacing (s) leads to an increase in
380 (δ_{em}/δ_p).

381 Thus, the settlement ratio (i.e., differential settlement) is substantially affected by the input
382 parameters; the pile and embankment modulii, embankment height (refer Figure 7a) and pile
383 spacing. A pile spacing equal to 2 m and 2.5 m follows the serviceability condition, which
384 means there is no differential settlement on the embankment surface.

385 ### *4.2 Soil arching ratio (SAR)*

386 The effect of pile modulus (E_p) and embankment modulus (E_{em}) is shown in Figure 10(a). The
387 *SAR* negligible effects with an increase in E_p. Further, *SAR* decreases (i.e., the tenancy of stress

388 transfer to pile increase) by up to 61 % with an increase in E_{em} from 15 to 30 MPa, which
389 implies that a specific value of E_{em} is required for maximum stress transfer to pile. The effect
390 of friction angle (ϕ') and dilation angle (ψ) is demonstrated in Figure 10(b). It shows that *SAR*
391 decreases up to 30 % with an increase in friction angle from 30° to 45° and the effect of dilation
392 angle is found to be negligible. However, *SAR* increases up to 7 % with an increase in dilation
393 angle, at the lower friction angle. Which means that soil arching increases with an increase in
394 ϕ'.

395 ### *4.3* Efficacy (E_{str})

396 The effect of pile modulus (E_p) and embankment modulus (E_{em}) on efficacy is shown in Figure
397 11(a). The effect of pile modulus on efficacy is found to be negligible, and efficacy increases
398 up to 87 % with an increase in embankment modulus. It implies that efficacy is dependent on
399 E_{em}, and it should be up to a specific value (25 MPa for this study) for maximum efficacy.
400 Figure 11(b) shows the effect of friction angle (ϕ') and dilation angle (ψ) on efficacy. It shows
401 that efficacy increases up to 20% with an increase in friction angle from 30° to 45° and the
402 effect of dilation is found to be negligible. Resulting, the effect of friction angle is more
403 pronounced as soil arching increases with an increase of ϕ'.

404 ### *4.4 Effect on arching height* (h_{arch})

405 The soil arching height is defined as the minimum height required for the development of full
406 soil arching. According to BS8006-1 [36], soil arching will occur when the embankment height
407 is equal to 1.4(s-d), whereas EBGEO [37] suggested 0.7l_d. where s is the centre to centre pile
408 spacing, d is the pile width, and l_d is the diagonal length.

409 The influence of the embankment height (h) on the height of the soil arch for different spacing
410 (s) is presented in Figure 12(a), which shows that the height of the soil arch (h_{arch}) is closely

411 related to h. For a specific s, it increases with an increase in h up to a certain height (5·0 m in
412 this study) and then remains constant beyond this critical embankment height. It can be verified
413 by Figures 4(a), 6(a), and 8(a) for s = 2.5 m.

414 The influence of the clear spacing between the piles (s-d) on the height of the soil arch for
415 different h can be observed in Figure 12(b). It is evident that (s-d) has a significant effect on
416 the height of the soil arch. For a specific h, (h_{arch}) has been found to increase with an increase
417 in (s-d) within the range from 1.5 to 3.5 m. It also shows that plot (h_{arch}) versus (s-d) are almost
418 the same trend when h is higher than its critical height (5m for this study).

419 The results of the (h_{arch}) plotted against the internal friction angle (ϕ') of the embankment fill
420 are given in Figure 12(c). It can be seen that (h_{arch}) increases with an increase in the ϕ' value.
421 When s = 2 m, the (h_{arch}) value is dramatically increased after 40° friction angle. The effect of
422 h and (s-d) on the arching height are consistent with Yang et al. [38] findings.

423 *4.5 Influence of train speed*

424 Figure 13 refers to the effect of vertical stress (σ_t) induced by a range of train speeds (V) on the
425 differential settlement and SAR. Figure 13(a) shows that the settlement ratio (δ_{em}/δ_p) increases
426 with an increase in h/(s-d) (due to reduction in s). The settlement ratio decreases with an
427 increase in train speed (V) for a given value of h/(s-d). As Table 3 indicates, the increased train
428 speed implies increased σ_t on the top of the railway embankment. The effect of vertical stress
429 (σ_t) is evident in Figure 13(b). It implies that for smaller pile spacing, SAR decreases with an
430 increase in train speed (i.e., the tenancy of stress transfer to pile increase). However, the effect
431 on SAR found to be negligible for larger pile spacing.

432 *4.6 Shape of soil arching*

433 A precisely defined soil arch shape is the essential requirement to perceive the soil arching
434 effect accurately. In the literature, some assumed arch shapes are used to develop the analytical
435 models of the soil arching effect. These models are summarized by Van Eekelen et al. [39] as
436 (a) rigid arch models, where the shape of the soil arch is assumed to be 2D or 3D triangular.
437 Additionally, it is assumed that the entire load above the soil arch is directly transferred to the
438 pile head, and the subsoil and reinforcements carry the weight of the soil below to the soil arch.
439 (b) Limit state equilibrium models: these models are based on the failure condition either at the
440 crown or the pile head of the soil arch. Commonly two limit-state equilibrium models are used
441 in piled embankment design. One is explained by Hewlett and Randolph [12] as the shape of
442 soil arch semicircular in 2D and a hemispherical dome in 3D which was adopted in the French
443 ASIRI guidelines and in the suggested BS8006-1 [36] and was recently extended by Zhang et
444 al. [23] by considering the triangular arrangement of the piles. The other is the multi-shell
445 arching theory models proposed by Kempfert et al. [40], in which a set of multi-shell domes
446 represent the soil arch. The multi-shell arching theory was adopted in the German guidelines
447 EBGEO [37] and Dutch guidelines. (c) Frictional models [9, 41]: In these models, the soil arch
448 had no definite shape and is considered the plane of equal settlement. Thus, the existing
449 analytical models of soil arching give a variation in the results for the same condition. One of
450 the primary reasons for this may be related to the assumed shape of the soil arch. Therefore,
451 the shape of the soil arch needs to be further evaluated. The effect of the input parameters on
452 the shape of the soil arch is illustrated in Figure 14.

453 To demonstrate the shape of arch inside the embankment fill, the vertical stress profile along
454 different vertical planes in the clear pile spacing (*s*-*d*) is used. The height of the maximum
455 vertical stress from the embankment base for individual planes is considered to be the height
456 of the outer boundary of the soil arch whereas the height of the minimum vertical stress
457 represents the inner boundary of the soil arch.

458 The vertical stress profile decreases at the height of 1.3 m [$h/(s\text{-}d) = 0.6$] above the base of the
459 embankment and then again starts to increase at the height of 0.54 m [$h/(s\text{-}d) = 0.25$] above the
460 embankment base. It means the thickness of the arch is about 0.76 m at the crown of the arch.
461 However, Hewlett and Randolph [12] and BS8006-1 [36] assumed that the shape of the arch is
462 semicircular with a uniform thickness which is equal to half of the pile head width. Thus, it
463 confirms that the shape of the soil arch is not semicircular. The shape of the arch is very similar
464 to the multi-shell arching theory proposed by Kempfert et al. [40]. The effect of the pile
465 modulus (E_p) on the arching shape is shown in Figure 14(a). The shape of the arch negligible
466 influenced at point A by increasing E_p. The effect of the embankment modulus (E_{em}) on the
467 shape of the arch is shown in Figure 14(b), showing that the shape of the arch increases by
468 increasing E_{em}. It may be concluded that E_{em} should be sufficient to develop soil arching. The
469 friction angle (ϕ') effect on the shape of the soil arch is evident in Figure 14(c). It implies that
470 a more stable arch can be formed by increasing ϕ' which is capable of transferring the maximum
471 load onto the pile. The effect of dilation angle (ψ) on the shape of the soil arch is illustrated in
472 Figure 14(d). It can be inferred that the thickness of the arch increases by increasing ψ. It may
473 have practical importance as the thickness of the soil arch increases.

474 ## 5. Comparison with design methods

475 Various analytical methods [9, 12, 36-37, 42] are available for piled embankment design. Table
476 5 summarizes the different equations used in various design methods to calculate soil arching
477 ratio (SAR) and efficacy (E_{str}). However, these design methods show variations in the arching
478 results due to the use of different analytical models. In this study, the soil arching ratio (SAR)
479 and efficacy (E_{str}) are compared using different analytical design methods for a range of
480 normalized embankment heights (h/s). The pile spacing (s) is fixed (2.5 m) whereas the
481 embankment height changes. Figure 15(a) shows the variation in soil arching ratio (SAR) using

these methods. It is observed in Figure 15(a) that the Guido method [42] is under-predicated. The Terzaghi [9] and BS8006 methods [36] are over-predicated. However, the Hewlett and Randolph method [12] shows nearly the same trend with an increase in embankment height. Figure 15(b) compares efficacy (E_{str}), showing that Terzaghi method [9] is very conservative. However, Hewlett and Randolph [12], and BS8006 [36] methods are shown closer prediction with higher embankment height. It also can be seen that for efficacy, Guido [42] shows the slightly higher result with all embankment height. Figure 15 confirms that the FE results are inconsistent with these methods. Also, different methods show the same trend in terms of soil arching which implies that each design method demonstrates soil arching in a certain term (i.e., *SAR* and E_{str}). Thus, there is a need to develop a method which could be considered globally for the design of a piled embankment.

6. Practical implications

Minimising differential settlement is the primary concern for the piled embankment design, and it has been acknowledged that soil arching help to reduce the differential settlement. In the literature, an optimum embankment height (h_{opt}) is introduced to account for soil arching beyond which differential settlement is minimal [5]. In this study, the height of soil arching is given in terms of clear pile spacing (*s*-*d*), which can be used to determine the optimum embankment height. The parametric study is useful to identify the most critical piled embankment parameters and their correlation with the conditions mobilizing soil arching. The practical implications of this study are as follows:

(i). The height of soil arching in the present study is summarized in Table 4, and it is verified with other published results. It is worth noting that in this study, the height of soil arching is 1.04 times of clear pile spacing (*s*-*d*), which is applicable to all considered pile spacing (i.e., 2.0 m, 2.5 m and 3.5 m). Above this embankment height, the uniform settlement is observed.

This implies that h_{opt} should be equal to 1.04 times of clear pile spacing (*s*-*d*) for complete mobilization of soil arching.

(ii). It is noteworthy to mention that soil arching is concerned with the optimum embankment height. However, FEM results of this study indicate that variations in the piled embankment parameters also have significant effects on the extent to which soil arching would be mobilized. Based on the parametric study results, it is evident that embankment modulus and friction angle play vital roles on the load transfer (e.g. soil arching) mechanism. Following relationships are established between soil arching ratio (*SAR*) and the embankment modulus and friction angle as below:

$$SAR = a\,(E_{em})^b + c \tag{10}$$

where, a, b, c are coefficients and the values are 1.331e+6, -6.079, and 0.2803, respectively.

$$SAR = -0.0061\phi' + 0.4791 \tag{11}$$

Therefore, this study is beneficial to identify optimum embankment height as a function of clear pile spacing, and the most critical design parameters to the optimize embankment design (refer to Eq. 10 and 11).

7. Limitations

Following are the limitation of this study which can be incorporated in future study:

(i). In this study, a linear elastic-perfectly plastic model with Mohr-Coulomb (MC) failure criterion was considered for soil. It is acknowledged that the use of the Mohr-Coulomb model can result in overprediction of strength at higher normal stresses. However, the expected normal stresses in a typical traffic scenario would not be too large. The low stress at embankment top is meant for the gravity loading analysis (self-weight of embankment). The

528 low stress condition is applicable to stress state in embankment top during train loading when
529 train-induced transient stresses attain peak values in the top layers of embankment. This is also
530 evident in past through fully instrumented field studies in Australia [22, 43]. In the present
531 study, the dynamic nature of train loading is not considered and hence the use of M-C model
532 was considered appropriate for the modeling. The use of M-C model is also consistent with
533 other past studies [27, 44]. Ye et al. [27] simulated embankment fill as linear elastic-perfectly
534 plastic model with Mohr-Coulomb (MC) failure criterion considering surcharge. Li et al. [44]
535 simulated a ballasted railway track with Mohr-Coulomb (MC) model for embankment
536 considering train speed from 100 km/h to 440 km/h.

537 (ii). The current study deals with the use of cohesive-frictional materials possessing high
538 frictional strength and coarse-grained soil for embankment fill and gravel bed which can largely
539 remain in a relatively dry state. The consolidation settlements are ignored in this study.
540 However, the consolidation can be significant issue when dealing with soft saturated subsoils.

541 ## 8. Conclusions

542 A numerical study on pile-supported railway embankment under the plane strain condition has
543 been presented in this paper. The soil arching behavior was investigated using the plane strain
544 model results. The study was further expanded to a parametric study to investigate the influence
545 on the size and shape of soil arching with varying piled-embankment parameters, pile spacing
546 and embankment height.

547 Based on the FE analysis, the following conclusions may be drawn from the present study:

548 • Arching was significantly affected by the piled railway embankment properties. Pile
549 and embankment modulii and friction angle were found to play a vital role in soil
550 arching behavior.

- The arch height was significantly affected by the embankment height and clear spacing between the piles and the friction angle.
- The soil arching significantly increases with a decrease in pile spacing. Thus, pile spacing should be limited for efficient load transfer to the piles.
- The shape of the soil arch is not semicircular with uniform thickness, rather, it follows the multi-arch theory. The formation of the soil arch starts from the lower boundary to the upper boundary. The shape and formation of the soil arch are still not understood well. Thus, more research is needed on the shape and formation of the soil arch, in particular.
- The comparison of the plane strain numerical results with the available design methods shows inconsistencies. Further research needs to be carried out in order to improve the available design and analytical methods.

ACKNOWLEDGMENTS

The authors gratefully acknowledge the financial support provided by the Government of India under the National Overseas Scholarship, No. 11016/16/2016 Education.

Reference

[1] Ma L, Shen S-L, Luo C-Y, Xu Y-S. Field Evaluation on the Strength Increase of Marine Clay under Staged Construction of Embankment. Mar Georesour Geotechnol 2001;29(4):317-332.

[2] Krishnamoorthy A, Kamal S. Stability of an Embankment on Soft Consolidating Soil with Vertical Drains. Geotech Geol Eng 2016;34(2):657-669.

[3] Saride S, Puppala AJ, Williammee R, Sirigiripet SK. Use of lightweight ECS as a fill material to control approach embankment settlements. J Mater Civ Eng 2009;22(6):607-617.

[4] Yi Y, Liu S, Puppala, AJ, Xi P. Vertical bearing capacity behaviour of single T-shaped soil-cement column in soft ground: laboratory modelling, field test, and calculation. Acta Geotech 2017;12(5):1077-1088.

[5] Lai H, Zeng J, Zang R, Cui M. Classification and characteristics of soil arching structures in pile-supported embankments. Comput Geotech 2018;98:153-171.

[6] Liu SY, Du YJ, Yi Y L, Puppala AJ. Field investigations on performance of T-shaped deep mixed soil cement column-supported embankments over soft ground. J Geotech Geoenviron Eng 2012;718-727.

[7] Fattah MY, Mohammed HA, Hassan HA. Load transfer and arching analysis in reinforced embankment. Proc Inst Civ Eng Struct Build 2016;169(11):797-808.

[8] Han J, Gabr MA. Numerical analysis of geosynthetic-reinforced and pile-supported earth platforms over soft soil. J Geotech Geoenviron Eng 2002;128(1):44-53.

[9] Terzaghi K. Theoretical soil mechanics. New York: John Wiley and Sons; 1943.

[10] Low BK, Tang SK, Choa V. Arching in piled embankments. J Geotech Eng 1993;120(11):1917-1938

[11] Han J, Wang F, Al-Naddaf M, Xu C. Progressive development of two-dimensional soil arching with displacement. Int J Geomech 2017;17(12):04017112.

[12] Hewlett WJ, Randolph MF. Analysis of piled embankments. Ground Eng 1988;21(3):12-18.

[13] Jenck O, Dias D, Kastner R. Three-dimensional numerical modeling of a piled embankment. Int J Geomech 2009;9(3):102-112.

[14] Ariyarathne P, Liyanapathirana DS, Leo CJ. (2012). Comparison of different two-dimensional idealizations for a geosynthetic reinforced pile-supported embankment. Int J Geomech 2012;13(6):754-768.

[15] Bhasi A, Rajagopal K. Numerical investigation of time dependant behaviour of geosynthetic reinforcement piled embankment. Int J Geotech Eng 2013;7(3):232-240.

[16] Li X, Miao Y, Cheng K. Soil Arching Effect Analysis via a Modified Finite Element Model Based on a Field Test. J Test Eval 2018;46(5):2218-2226.

[17] Briançon L, Simon B. Performance of pile-supported embankment over soft soil: full-scale experiment. J Geotech Geoenviron Eng 2012;138(4):551-561.

[18] Nunez MA, Briançon L, Dias D. Analyses of a pile-supported embankment over soft clay: Full-scale experiment, analytical and numerical approaches. Eng Geol 2013;153:53-67.

[19] Fagundes DdF, Almeida MdeSde, Girout R, Blanc M, Thorel L. Behaviour of piled embankment without reinforcement. Proc Inst Civ Eng Geotech Eng 2015;168(GE6):514-525.

[20] Han J, Wang F, Al-Naddaf M, Xu C. Progressive development of two-dimensional soil arching with displacement. Int J Geomech 2017;17(12):04017112.

612 [21] Sun, QD, Indraratna B, Nimbalkar, S. Effect of cyclic loading frequency on the permanent
613 deformation and degradation of railway ballast. Géotechnique 2014;64(9):746-751.

614 [22] Nimbalkar S, Indraratna B. Improved performance of ballasted rail track using
615 geosynthetics and rubber shockmat. J Geotech Geoenviron Eng 2016;142(8):04016031.

616 [23] Zhang C, Jiang G, Liu X, Buzzi O. Arching in geogrid-reinforced pile-supported
617 embankments over silty clay of medium compressibility: Field data and analytical solution.
618 Comput Geotech 2016;77(7):11-25.

619 [24] Huang J, Han J. Two-dimensional parametric study of geosynthetic-reinforced column-
620 supported embankments by coupled hydraulic and mechanical modeling. Comput Geotech
621 2010;37(5):638-648.

622 [25] Abaqus 6.13 Online Documentation, Abaqus Analysis User's Manual C Dassault
623 Systèmes, Hibbit, Karlsson and Sorensen Inc., RI, USA, 2013. [accessed July 2019].

624 [26] Esmaeili M, Arbabi B. Railway embankments stabilization by tied back-to-back system.
625 Comput Geotech 2015;67:110-120.

626 [27] Ye GB, Wang M, Zhang Z, Han J, Xu C. Geosynthetic-reinforced pile-supported
627 embankments with caps in a triangular pattern over soft clay. Geotext Geomembr
628 2020;48(1):52-61.

629 [28] Potyondy JG. Skin friction between various soils and construction materials.
630 Géotechnique 1961;11(4):339-353.

631 [29] Yu Y, Bathurst RJ, Damians IP. Modified unit cell approach for modelling geosynthetic-
632 reinforced column-supported embankments. Geotext Geomembr 2016;44(3):332-343.

633 [30] Pham HV, Dias D. 3D Numerical Modeling of a Piled Embankment under Cyclic Loading.
634 Int J Geomech 2019;19(4):04019010.

635 [31] King L, Bouazza A, Dubsky S, Rowe RK, Gniel, J, Bui HH. Kinematics of soil arching in
636 piled embankments. Géotechnique 2019;1-18.

637 [32] Doyle NF. Railway track design: A review of current practice. Australian Government
638 Publishing Service, Canberra; 1980.

639 [33] Esveld C. Modern railway track. Zaltbommel, Netherlands: MRT-productions; 2001.

640 [34] Zhuang Y, Ellis EA, Yu HS. Plane strain FE analysis of arching in a piled embankment.
641 Proc Inst Civ Eng Ground Improv 2010;163(4):207-215.

642 [35] Potts VJ, Zdravkovic L. Finite element analysis of arching behaviour in soils. 12th
643 International Conference on Computer Methods and Advances in Geomechanics 2008;3642-
644 3649.

645 [36] British Standards Institution, BS8006. Code of practice for strengthened/reinforced soils
646 and other fills. British Standards Institution, London; 2010.

[37] German Standard, EBGEO. Recommendations for design and analysis of earth structures using geosynthetic reinforcements. German Geotechnical Society, Berlin, Germany; 2011.

[38] Yang T, Lu Z, Ni J, Wang G. 3D FE modeling of soil arch shape in a piled embankment. Proc Inst Civ Eng Geotech Eng 2018;1-8.

[39] Van Eekelen SJM, Bezuijen A, Van Tol AF. Validation of analytical models for the design of basal reinforced piled embankments. Geotext Geomembr 2015;43(1):56-81.

[40] Kempfert HG, Göbel C, Alexiew D, Heitz C. German recommendation for reinforced embankments on pile-similar elements. Proc 3rd European Geosynthetics Conf Munich, Germany 2004;279-284.

[41] McKelvey JA. (1994). The anatomy of soil arching. Geotext Geomembr 1994;13(5):317-329.

[42] Guido VA, Kneupel JD, Sweeny MA. Plate load testing on geogrid reinforced earth slabs. Proc Geosynthetics Conf 1987;216-225.

[43] Indraratna B, Nimbalkar S, Christie D, Rujikiatkamjorn C, Vinod J. Field assessment of the performance of a ballasted rail track with and without geosynthetics. J Geotech Geoenviron Eng 2010;136(7):907-917.

[44] Li L, Nimbalkar S, Zhong R. Finite element model of ballasted railway with infinite boundaries considering effects of moving train loads and Rayleigh waves. Soil Dyn Earthquake Eng 2018;114:147-153.

LIST OF TABLES:

TABLE 1. Material parameters for Piled embankment

Material	Unit weight, γ (kN/m^3)	Young's modulus, E (MPa)	Poisson's ratio, v	Cohesion c'(kPa)	Friction angle, ϕ'(degree)	Dilation angle, ψ(degree)
Pile	24	**20 × 10^3** (15 × 10^3 - 30 × 10^3)	0.15	-	-	-
Embankment fill	20	**20** (15 - 30)	0.25	0.1	**30** (30 - 45)	**0** (0 - 15)
Gravel bed	21	25	0.25	0.1	35	5
Subsoil	18.4	10	0.3	8	22	0

Note: bold values are for standard case (h = 3.5 m and s = 2.5 m)

Table 2. Dynamic Amplification Factor (DAF or Φ) calculation with different methods

Method	Equation	Train speed, V (km/h)	DAF	Remarks
AREA[1]	$\Phi = 1 + \frac{0.00521 \cdot V}{D_w}$ where, D_w = 0.97	40 60 80 100 120 140 160	1.21 1.32 1.43 1.54 1.64 1.75 1.86	D_w is the diameter of wheel (m)
Eisenmann	$\Phi = 1 + \delta\eta t$ where, δ =0.2 (for good track condition); t =1; $\eta = 1$; for V< 60 km/h $\eta = \left(1 + \frac{V-60}{140}\right)$; for 60 ≤ V ≤ 200 km/h	40 60 80 100 120 140	1.20 1.20 1.23 1.26 1.29 1.31	δ is a factor that depends on the track condition; t is a factor that depends on the upper confidence limit; η is factor that depends on the speed of the vehicle

		160	1.34	
ORE[2]	$\Phi = 1 + \alpha' + \beta' + \gamma'$ where, $\alpha' = 0.04\left(\frac{V}{100}\right)^3$; $\beta' = \frac{V^2(2h+h_s)}{127 R_c l_g} - \frac{2h_s h}{l_g^2}$; $\gamma' = \gamma_o \cdot a_o \cdot b_o$; $\gamma_o = 0.1 + 0.017\left(\frac{V}{100}\right)^3$	40 60 80 100 120 140 160	1.30 1.30 1.31 1.33 1.36 1.40 1.45	α' is a coefficient that depends on the track irregularities, train suspension, and speed; β' is a coefficient that accounts for the movement of train along a curve, γ' is a coefficient that depends on the train speed and configuration, and track condition; h_d is the cant/super-elevation deficiency (m), l_g is the gauge width (m), h is the vertical distance from rail top to centre of gravity of train (m), h_s is the super-elevation (m), R_c is the radius of curvature (m), a_o and b_o are the locomotive and track maintenance factors.
Japanese Standard	$\Phi = \left(1 + 0.3 \cdot \frac{V}{100}\right)(1 + C)$ where, $C \approx 0.3$	40 60 80 100 120 140 160	1.46 1.53 1.61 1.70 1.77 1.84 1.92	C is a coefficient
British Railways	$\Phi = 1 + \frac{8.784(\theta_1 + \theta_2)V}{P_0}\left(\frac{K_j W_u}{g}\right)^{0.5}$ where, $(\theta_1 + \theta_2) = 0.005$; $K_j = 55$; $W_u = 2.11 \times 9.81$; $g = 9.81$	40 60 80 100 120 140 160	1.20 1.29 1.38 1.48 1.58 1.67 1.77	$(\theta_1 + \theta_2)$ is the total dip angle of the rail joint (radians); K_j is the track stiffness at joint (kN/mm); W_u is the unsprung weight at one wheel (kN); g is the acceleration due to gravity (m/s^2).
Indian Railways	$\Phi = 1 + \frac{V}{58.14(k)^{0.5}}$ where, $k = 60$	40 60 80 100 120 140 160	1.08 1.13 1.18 1.22 1.27 1.31 1.36	k is the track modulus (MPa)
South African formula	$\Phi = 1 + \frac{4.92 \cdot V}{D_{w1}}$	40 60 80 100	1.20 1.30 1.40 1.50	D_{w1} is the diameter of wheel (mm)

	where, D_{w1} = 970	120	1.60	
		140	1.71	
		160	1.81	
WMATA[3]	$\Phi = (1 + 0.0001{V_o}^2)^{0.67}$ where, $V_o = V \times 0.621371$	40	1.04	V_o is the speed of train (miles/h)
		60	1.09	
		80	1.16	
		100	1.24	
		120	1.34	
		140	1.46	
		160	1.58	
Chinese Standard (MORPRC, 2009)	$\Phi = 1 + \alpha V$ where, α = 0.003	40	1.12	-
		60	1.18	
		80	1.24	
		100	1.30	
		120	1.36	
		140	1.42	
		160	1.48	
German formula	(i) $\Phi = 1 + \frac{V^2}{3\times10^4}$; for $V \leq 100$ km/h (ii) $\Phi = 1 + \frac{4.5\,V^2}{10^5} - \frac{1.5\,V^3}{10^7}$; for $V > 100$ km/h	40	1.06	-
		60	1.13	
		80	1.21	
		100	1.30	
		120	1.39	
		140	1.47	
		160	1.54	
Australian Standard (AS1085.14, 2012)	$\Phi = 2.5$	-	2.5	This value of Φ may be taken when the data from field investigations is unavailable.

[1]American Railway Engineering Association

[2]Office for Research and Experiments

[3]Washington Metropolitan Area Transit Authority

675 **TABLE 3.** Summary of Induced vertical stress on embankment obtained using Trapezoidal method

Stress calculation method	Impact factor calculation method	Vehicle speed, V (km/h)	Vertical stress on subgrade, σ_t (kPa)
Trapezoidal approximation (2:1 method)	ORE method	40	105
		60	106
		80	107
		100	108
$[\sigma_{z\,max} = \frac{Q}{(b+\hat{h})(\frac{l}{3}+\hat{h})}]$	$[\Phi = 1+\alpha'+\beta'+\gamma']$	120	110
		140	114
		160	118

676 where, $Q = \sigma_{max}$ (A_{sb}), l is sleeper length (m), α' and β' are related to the mean value of impact factor while γ' is related to the standard deviation of the impact
677 factor.

678

679 **TABLE 4.** Soil arching height verified by various studies

	Terzaghi [9]	Bhasi and Rajagopal [15]	Zhuang et al. [34]	Potts and Zdravkovic [35]	Present study
Normalized length	Void width	(*s*-*d*)	(*s*-*d*)	Void width	(*s*-*d*)
Soil arching height in Plane strain	2-3	2.9	3	3	2.25

680 **Note:** All values in meter

681

682 **TABLE 5.** Equations for calculating soil arching ratio (*SAR*) and efficacy (E_{str}) by different design methods

Design method	Soil arching ratio (*SAR*)	Efficacy (E_{str})
Terzaghi [9]	$SAR = \frac{(s^2-d^2)}{4hdK\,tan\phi'}(1-e^{(-4hdK\,tan\phi')/(s^2-d^2)})$	$E_{str} = 1-\frac{(SRR)(s^2-d^2)}{s^2}$

	where, $K = (1-\sin\phi')$	
Hewlett and Randolph [12]	**At the crown:** $SAR = \left(1-\frac{d}{s}\right)^{(2K_p-1)}\left(1-\frac{2s(K_p-1)}{\sqrt{2}h(2K_p-3)}\right)+\left(\frac{2(s-d)(K_p-1)}{\sqrt{2}h(2K_p-3)}\right)$ **At the pile top:** $SAR = \left(\frac{1}{\left(\frac{2K_p}{K_p+1}\right)\left[\left(1-\frac{d}{s}\right)^{(1-K_p)}-\left(1-\frac{d}{s}\right)\left(1+\frac{d}{s}K_p\right)\right]+(1-\frac{d^2}{s^2})}\right)$ where, $K_p = \frac{(1+\sin\phi')}{(1-\sin\phi')}$	
BS8006 [36]	**For partial Arching:**	
	$SAR = \frac{2s}{(s+d)(s^2-d^2)}\left[s^2-d^2\left(\frac{P_c}{\gamma h}\right)\right]$	$E_{str} = 1-\frac{1}{s^2}\left[s^2-d^2\left(\frac{P_c}{\gamma h}\right)\right]$
	For full arching:	
	$SAR = \frac{2.8s}{(s+d)^2h}\left[s^2-d^2\left(\frac{P_c}{\gamma h}\right)\right]$ where, $\left(\frac{P_c}{\gamma h}\right) = \left[\frac{C_c d}{h}\right]^2$	$E_{str} = 1-\frac{1.4(s-d)}{s^2h}\left[s^2-d^2\left(\frac{P_c}{\gamma h}\right)\right]$
Guido [42]	$SAR = \frac{(s-d)}{3\sqrt{2}\,h}$	

where, s is pile spacing, d is pile width, h is the embankment height, and K is the lateral stress coefficient at rest (K_o), K_p is the passive lateral stress coefficient, ϕ' is friction angle of embankment fill, C_c is the arching coefficient, P_c is vertical stress on the pile head and γ is the unit weight of embankment fill.

687 **LIST OF FIGURES:**

712

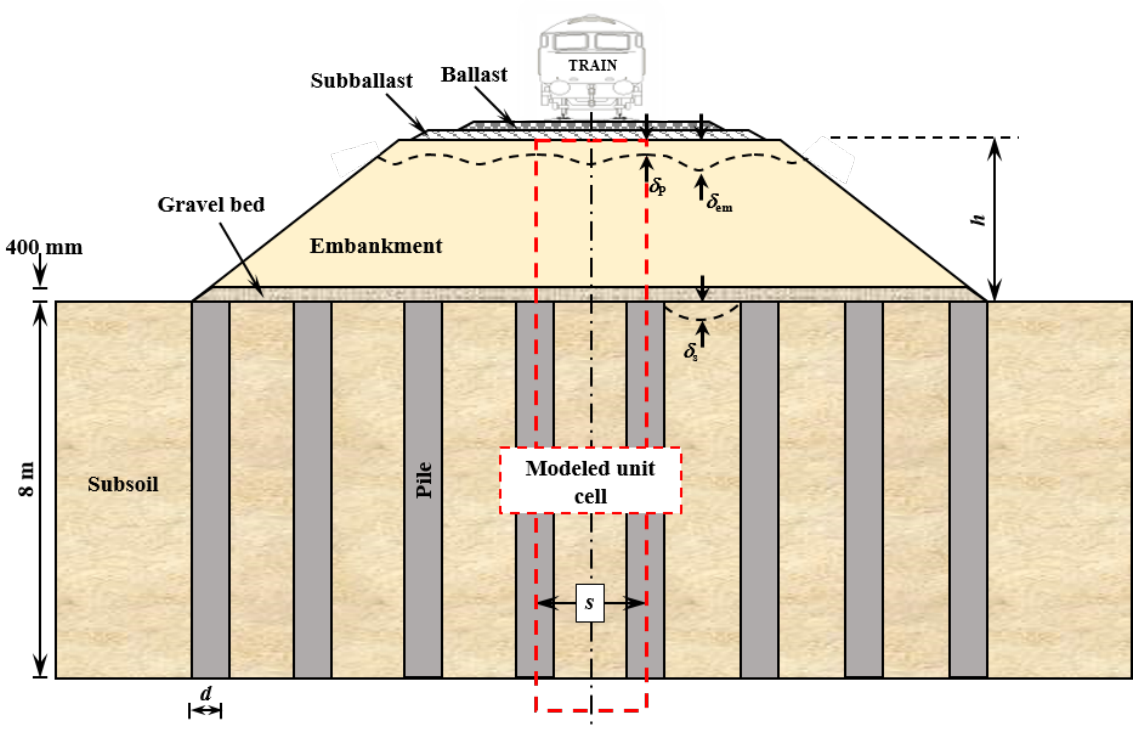

(a)

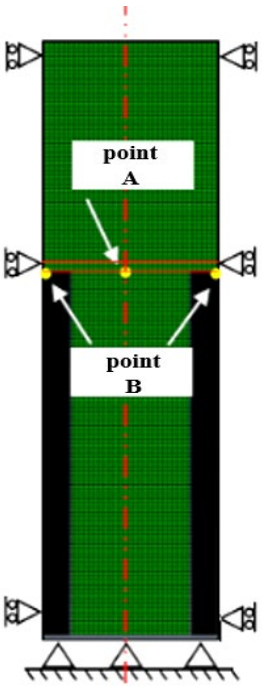

(b)

Figure 1: Considered embankment model, (a) typical cross-section profile, and (b) mesh profile of the modeled unit (s = 2.5 m, h = 3.5 m)

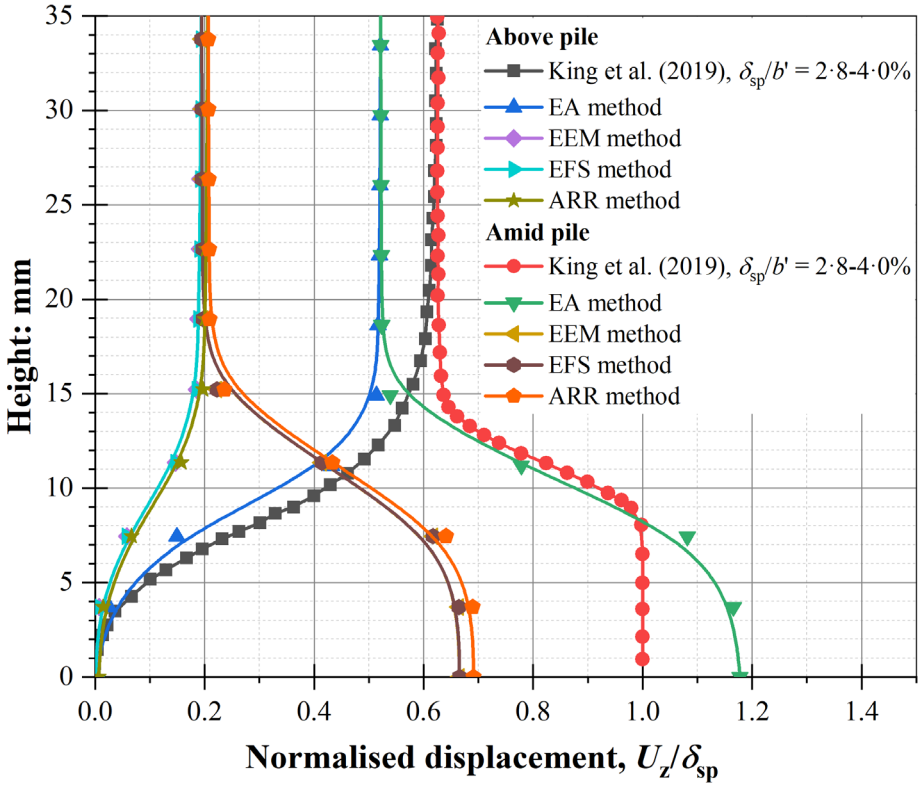

720

721 **Figure 2:** Model validation with experimental data reported by King et al. [31]

722

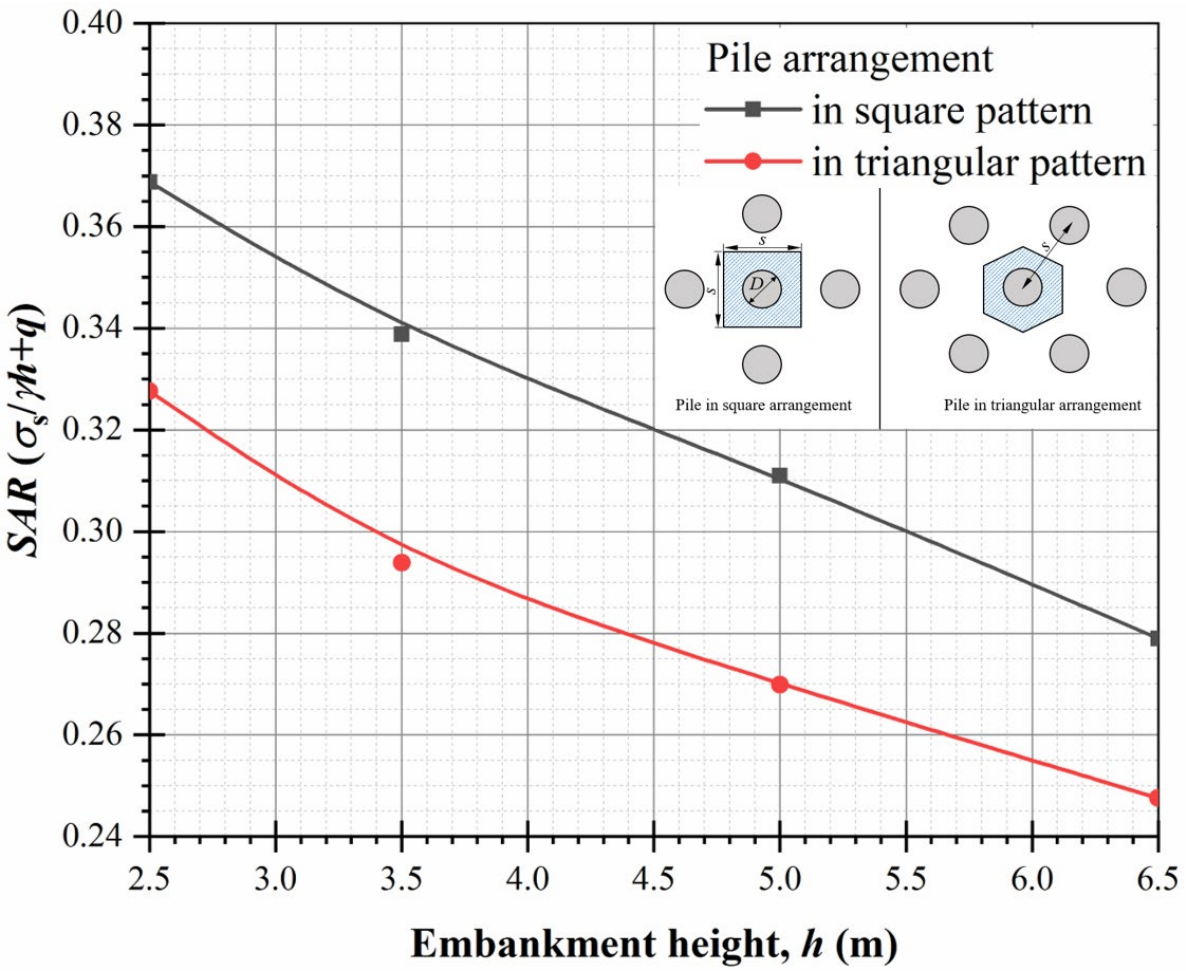

723

724 **Figure 3:** Comparison of two different pile arrangements

725

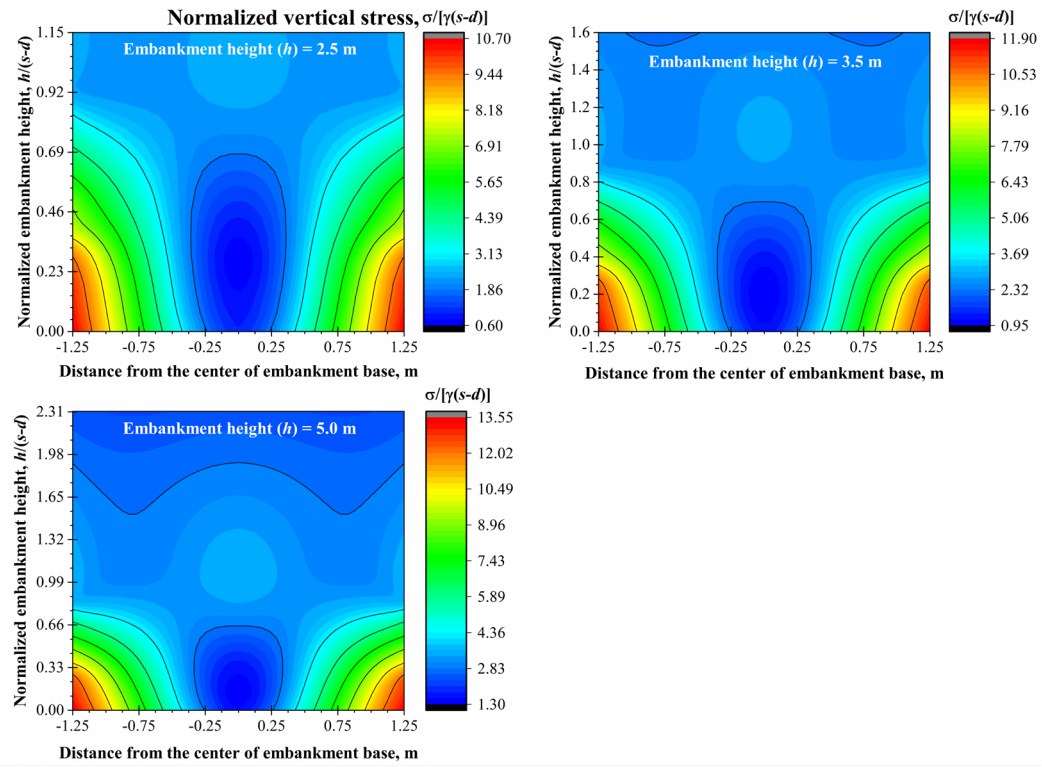

(a)

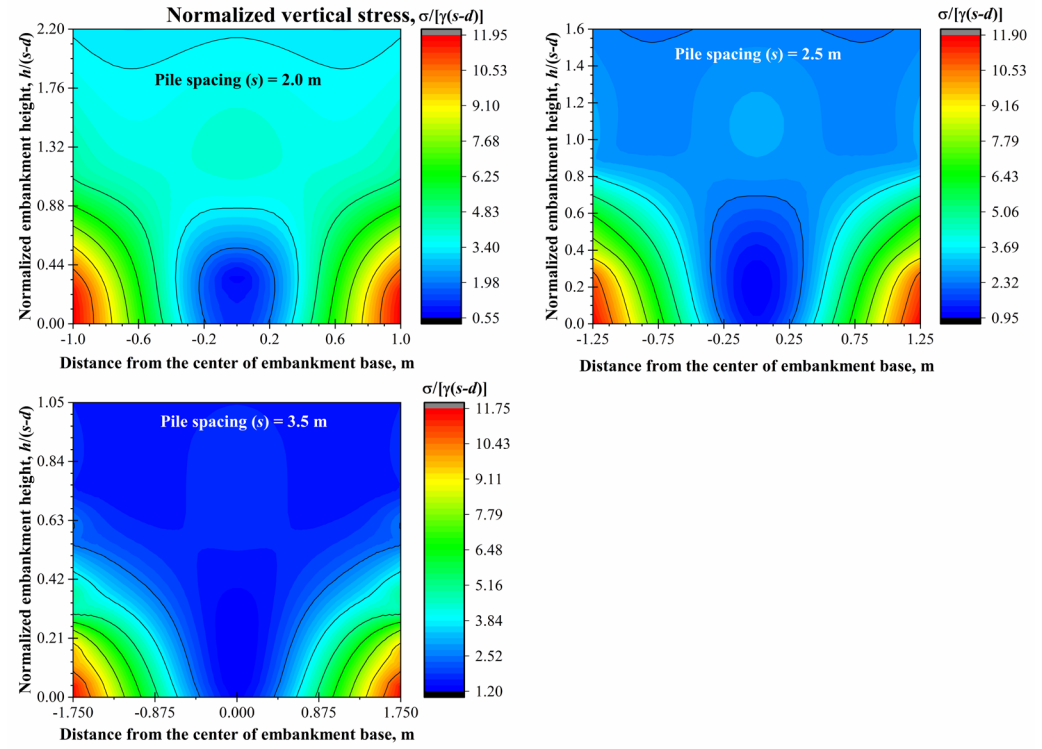

(b)

Figure 4: Vertical stress contour for varied; (a) embankment height, and (b) pile spacing

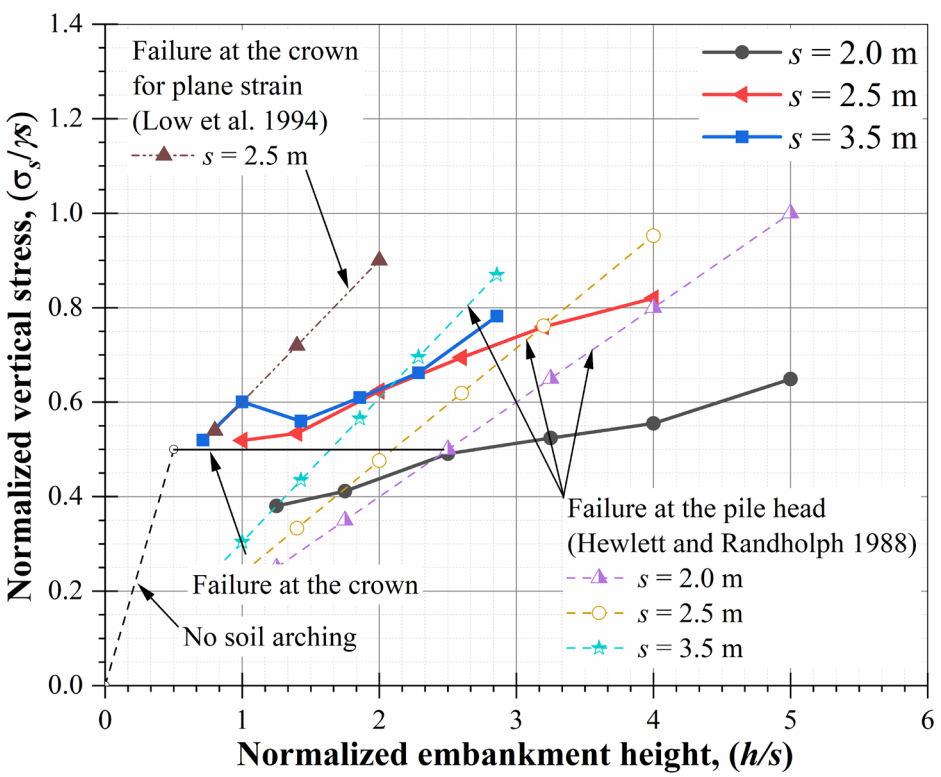

732

733 **Figure 5:** Comparison of FE results with Hewlett and Randolph method: normalized stress

734 on point A vs. normalized embankment height

735

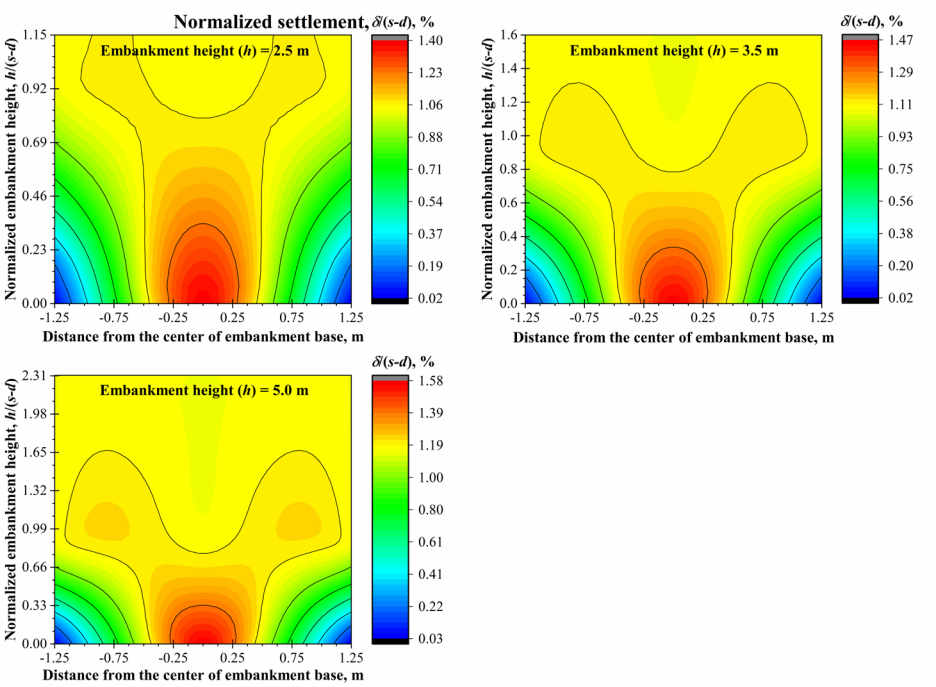

(a)

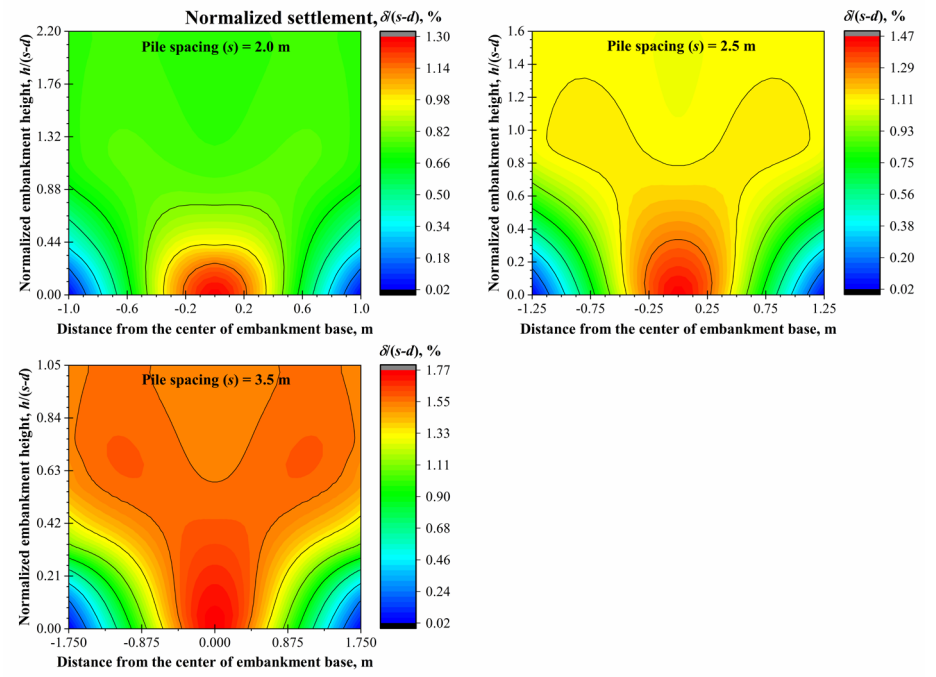

(b)

Figure 6: Normalized settlement contour for varied (a) embankment height, and (b) pile spacing

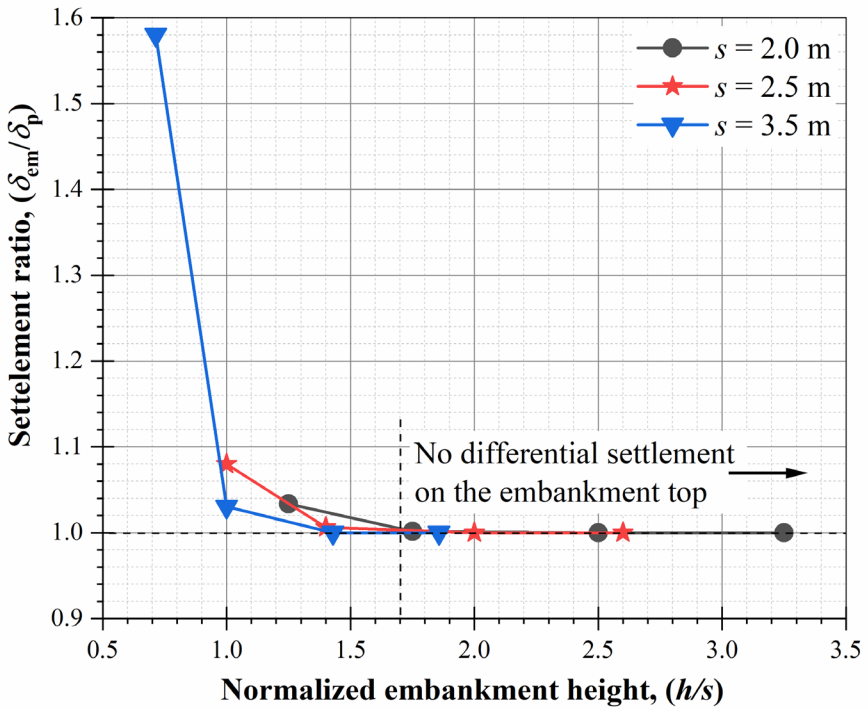

743

744 **(a)**

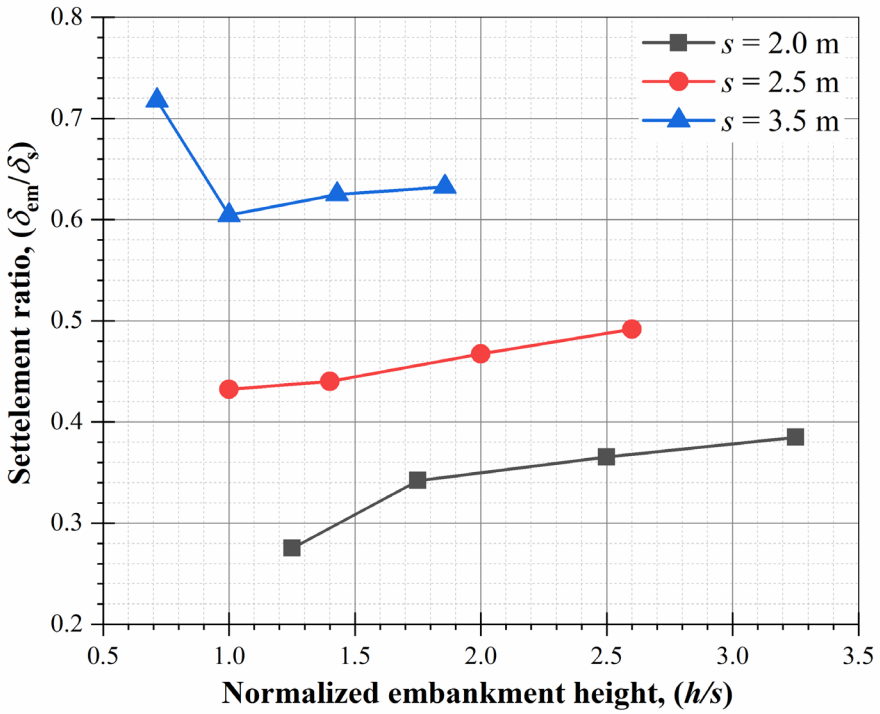

745

746 **(b)**

747 **Figure 7:** (a) Settlement ratio at the embankment top, (b) settlement ratio at point A

748

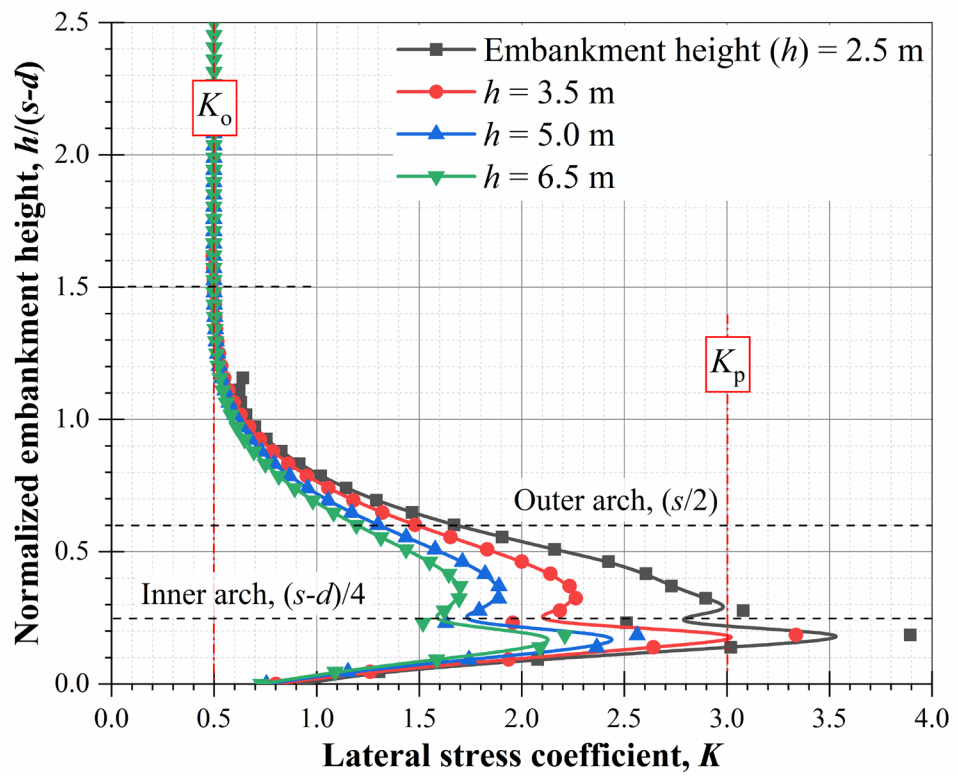

749

750 **(a)**

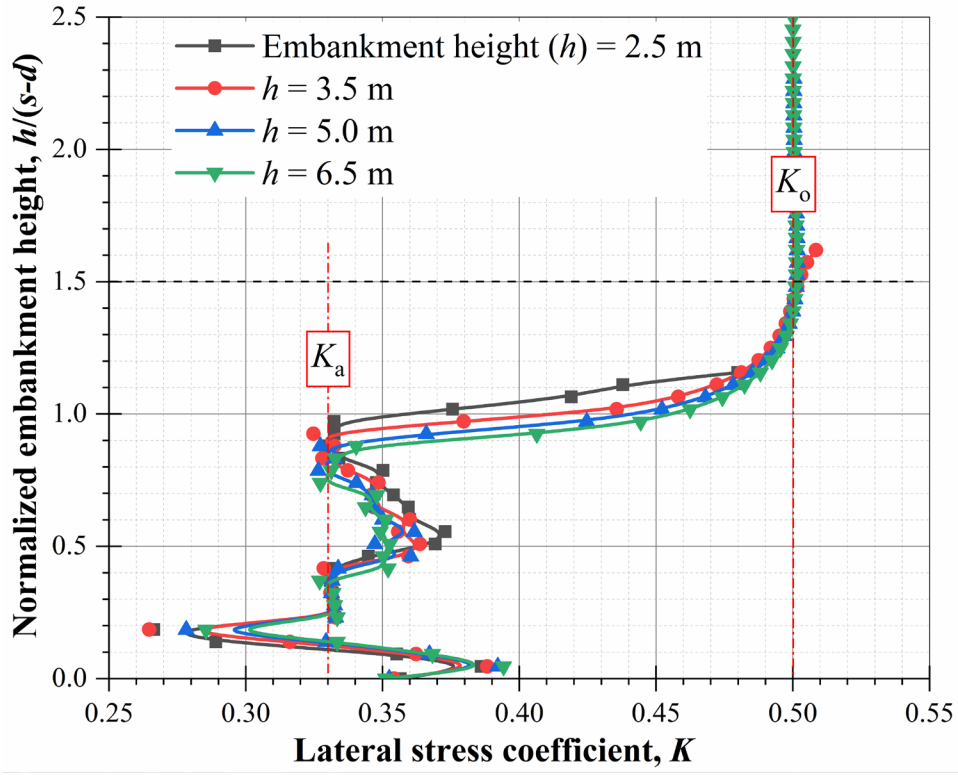

751

752 **(b)**

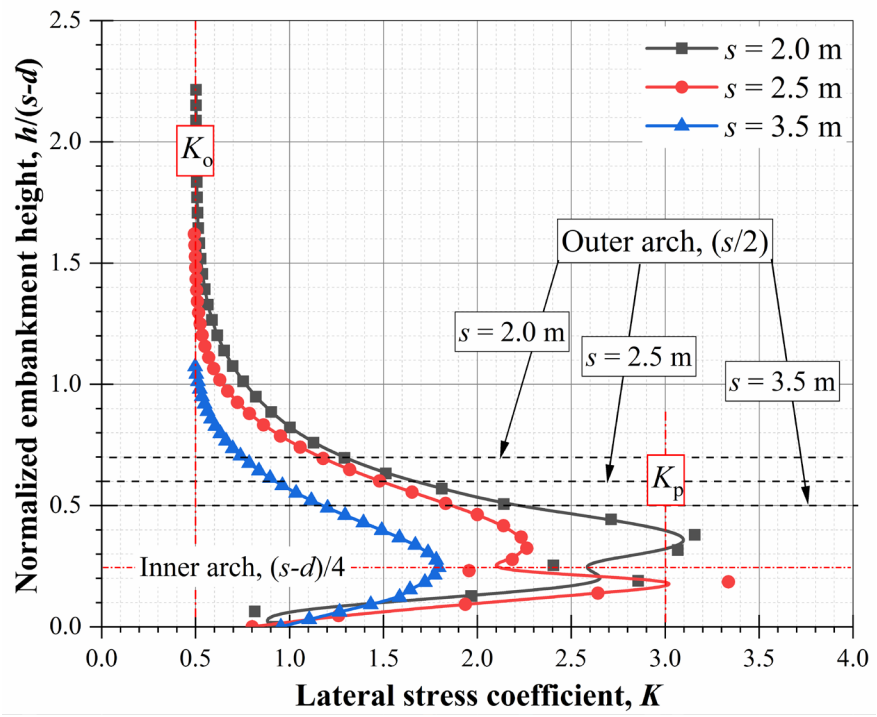

753

754 **(c)**

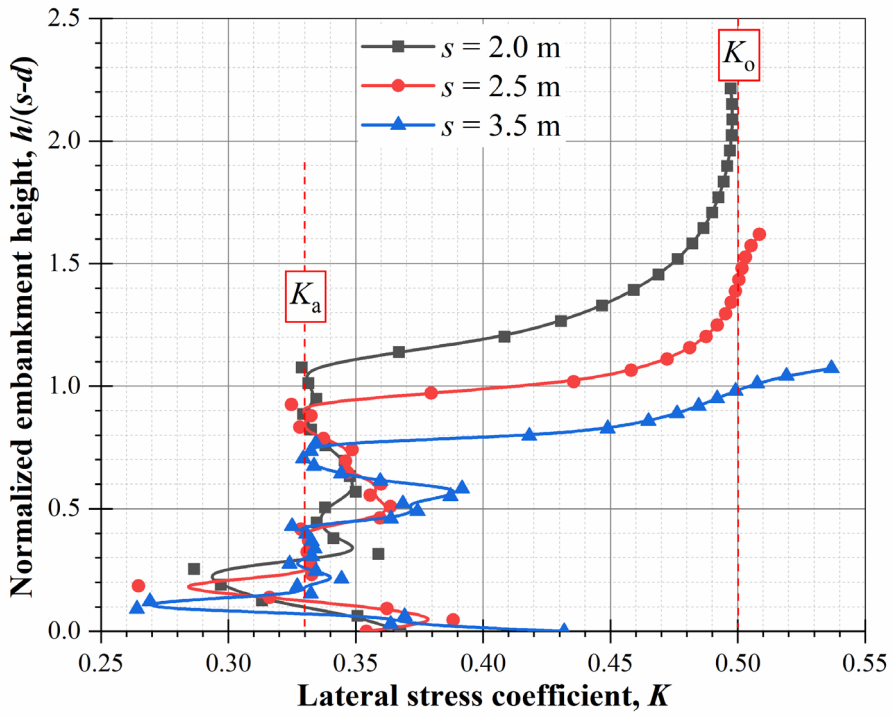

755

756 **(d)**

757 **Figure 8:** Lateral stress coefficient (*K*) profile for varied; embankment height (a) at point

758 A, (b) at point B, and pile spacing (c) at the point A, (d) at the point B

759

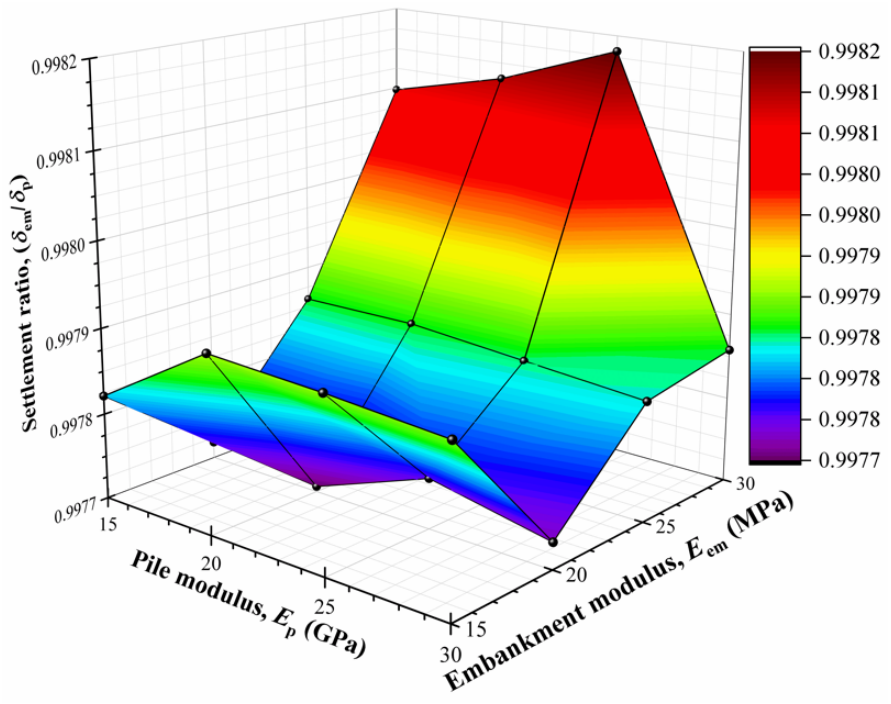

760

761 **(a)**

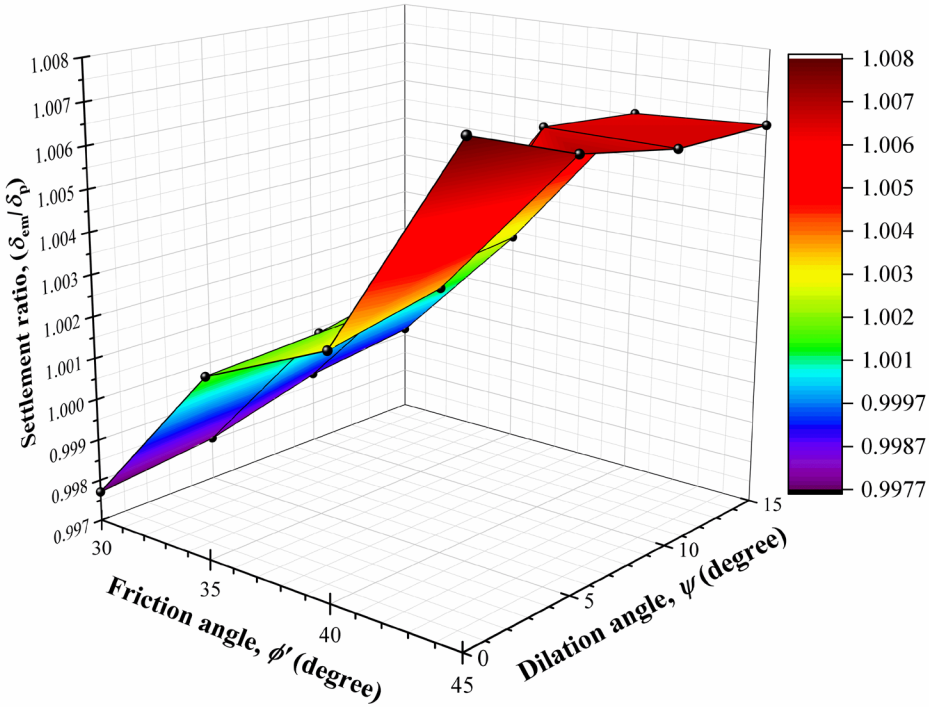

762

763 **(b)**

764 **Figure 9:** Influence on settlement ratio (δ_{em}/δ_p) due to (a) pile modulus and embankment

765 modulus (b) friction angle, and dilation angle

766

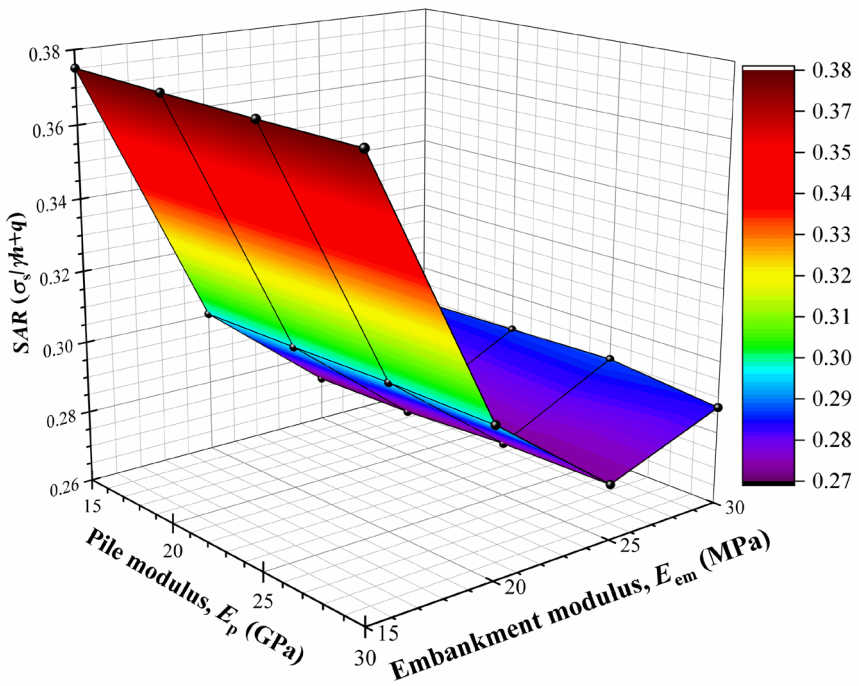

(a)

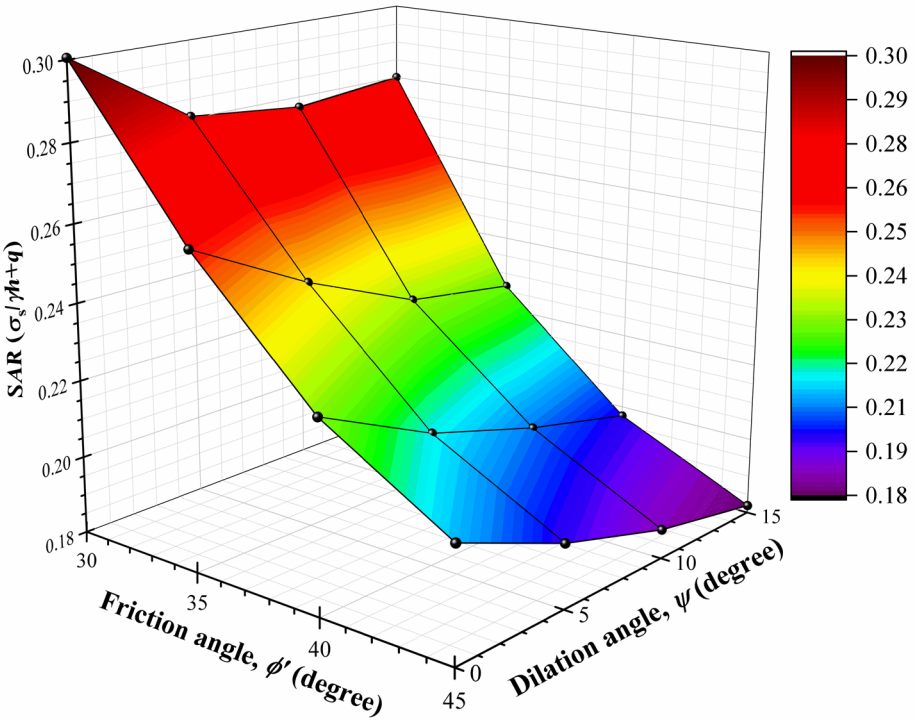

(b)

Figure 10: Influence on soil arching ratio (*SAR*) due to (a) pile modulus and embankment modulus, (b) friction angle and dilation angle

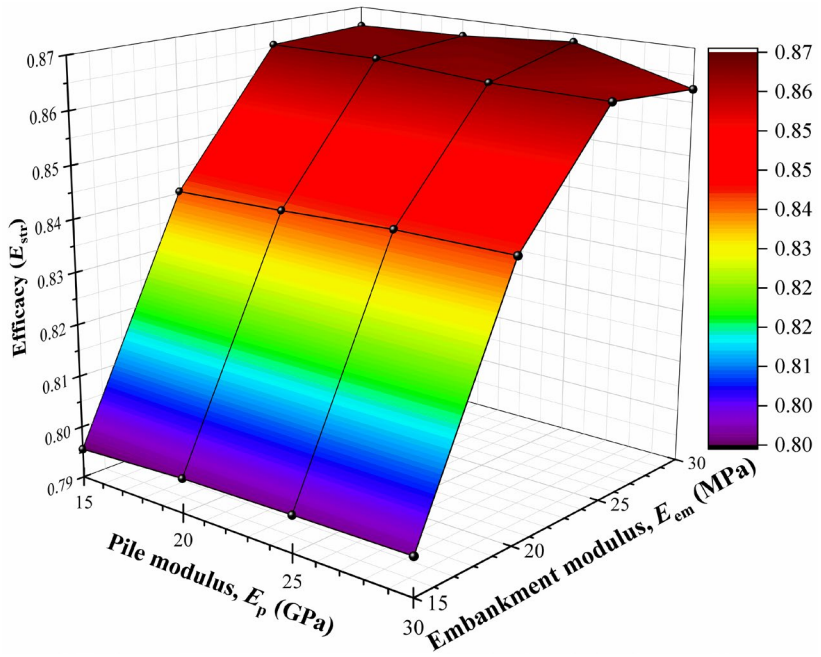

774

775 **(a)**

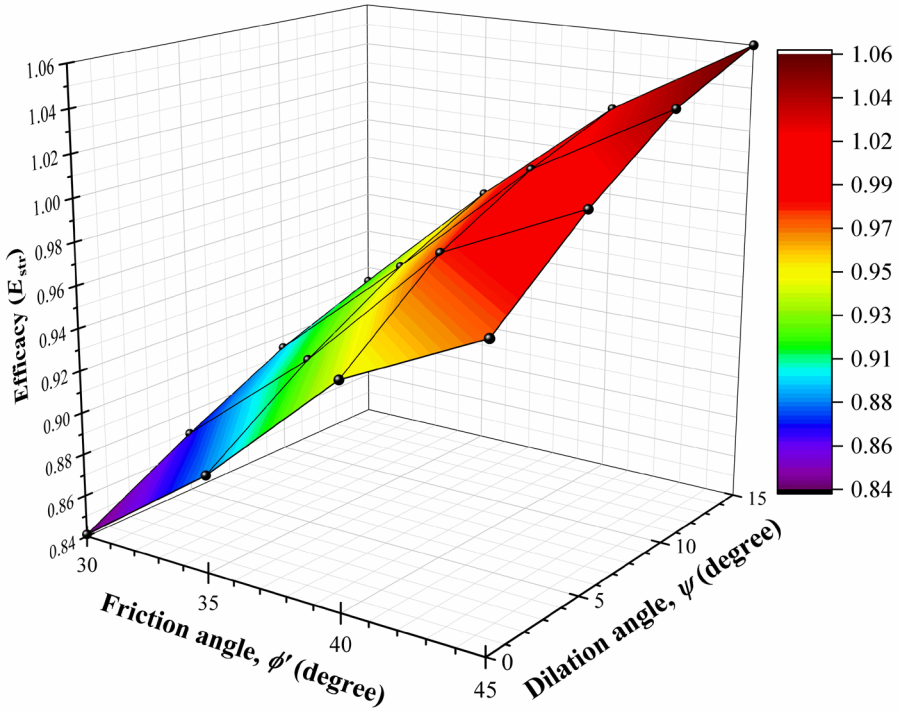

776

777 **(b)**

778 **Figure 11:** Influence on efficacy (E_{str}) due to (a) pile modulus and embankment modulus (b)

779 friction angle and dilation angle

780

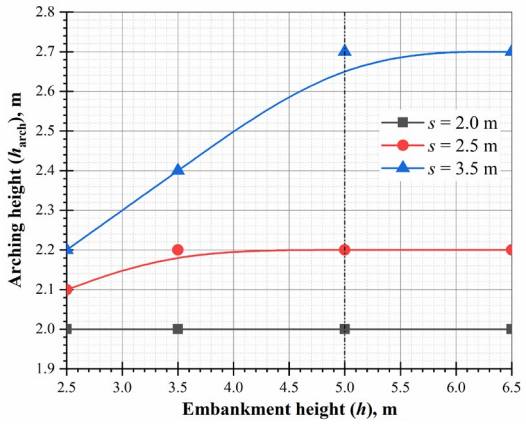

781

782 **(a)**

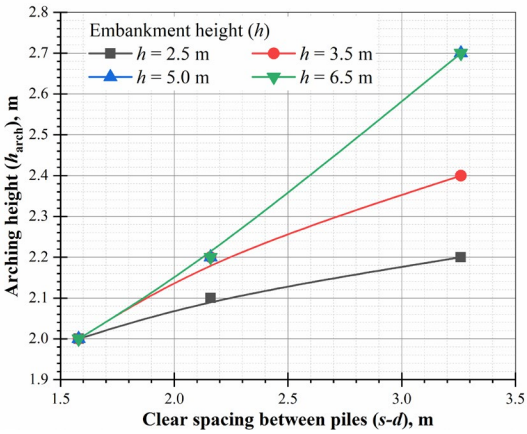

783

784 **(b)**

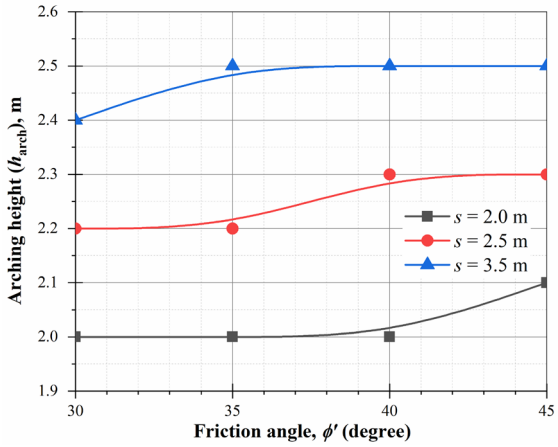

785

786 **(c)**

787 **Figure 12:** Influence on arching height (h_{arch}) due to (a) embankment height, (b) pile spacing

788 (s-d), and (c) friction angle

789

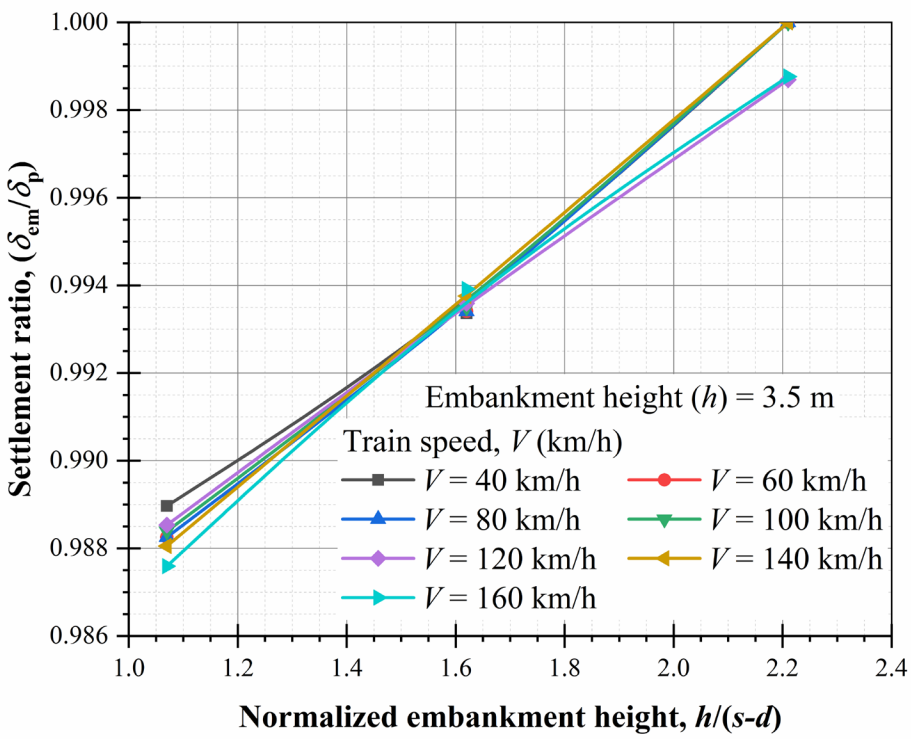

790

791 **(a)**

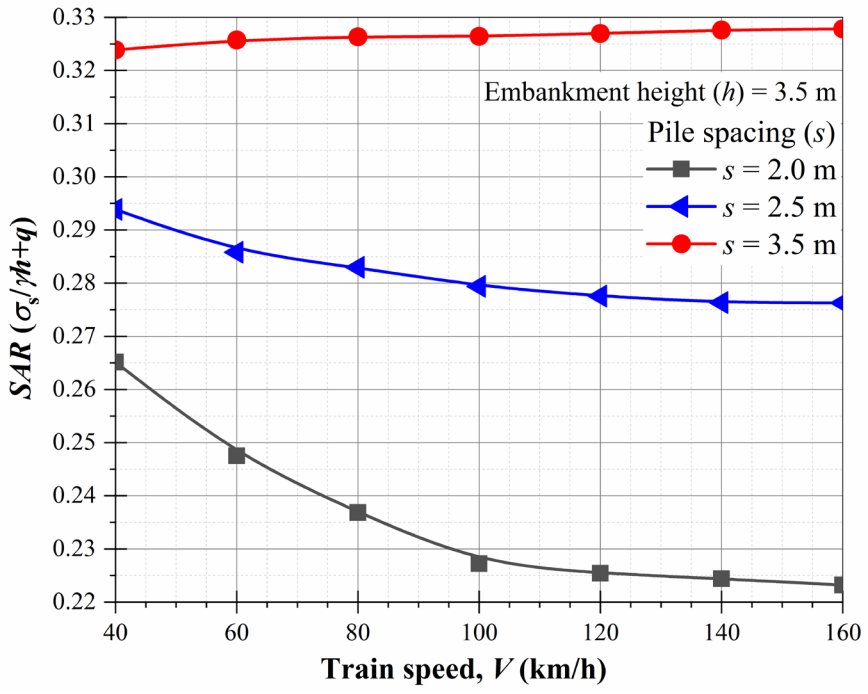

792

793 **(b)**

794 **Figure 13:** Influence of train speed on (a) settlement ratio, (b) soil arching ratio (*SAR*)

795

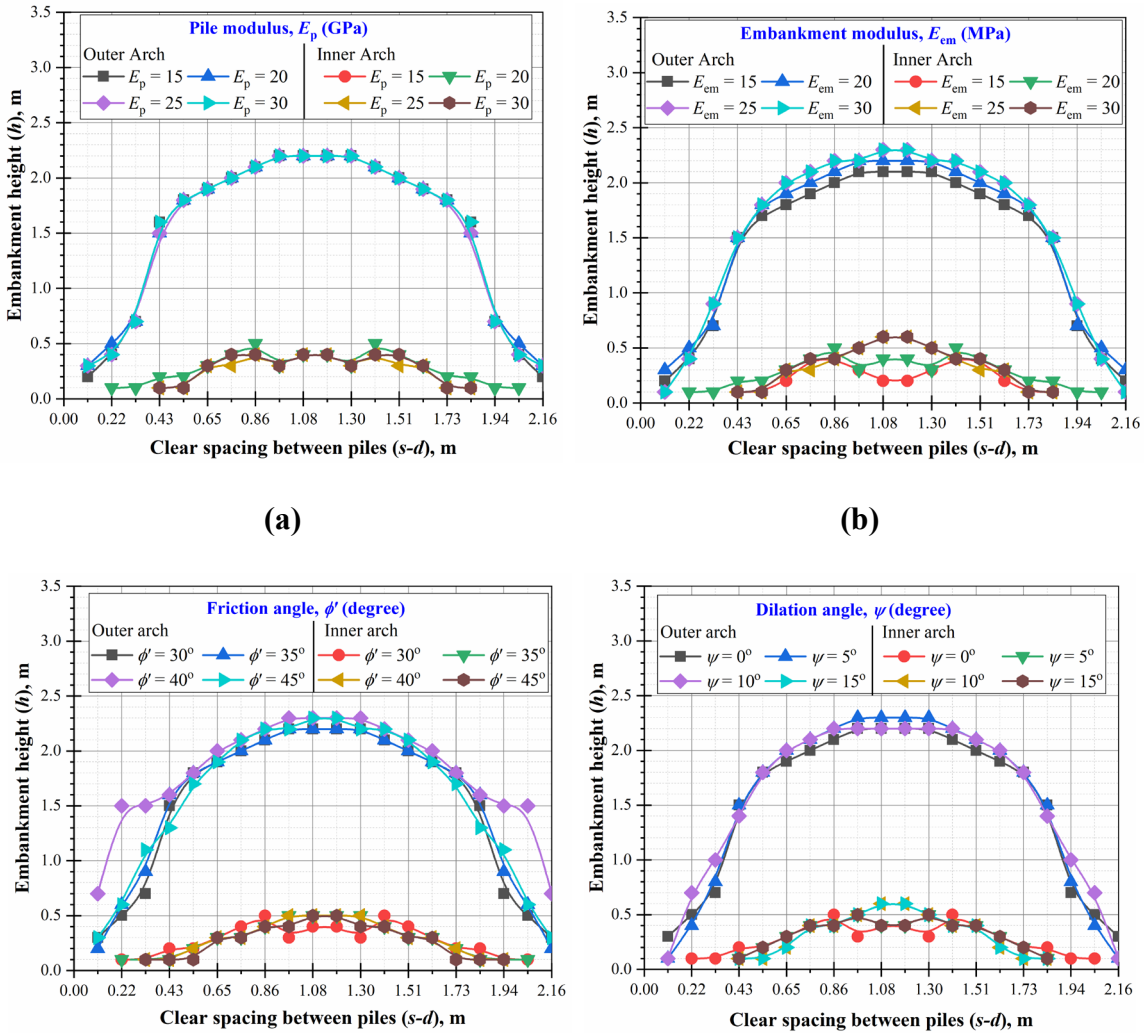

Figure 14: Influence on arching shape due to (a) pile modulus, (b) embankment modulus, (c) friction angle, and (d) dilation angle

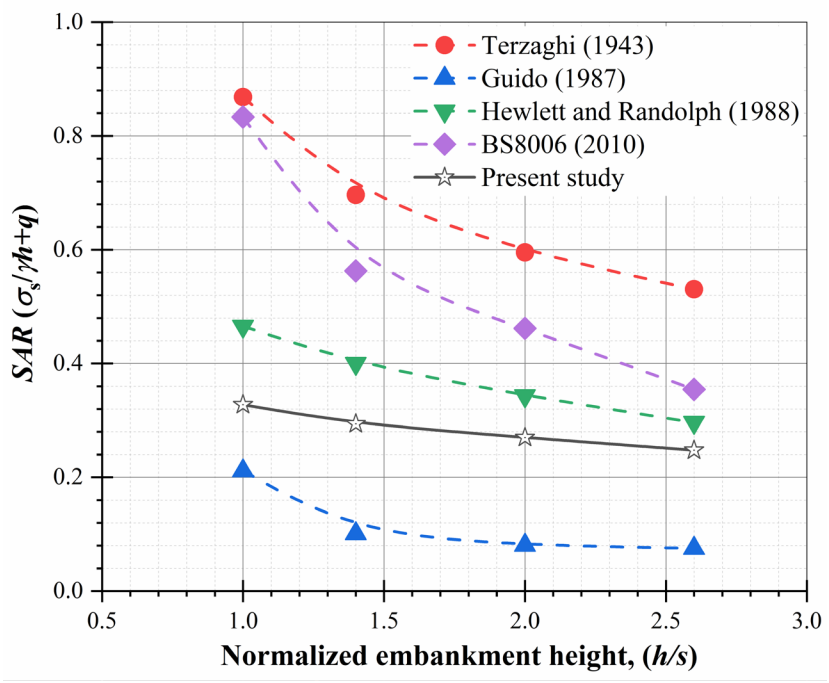

803

804 **(a)**

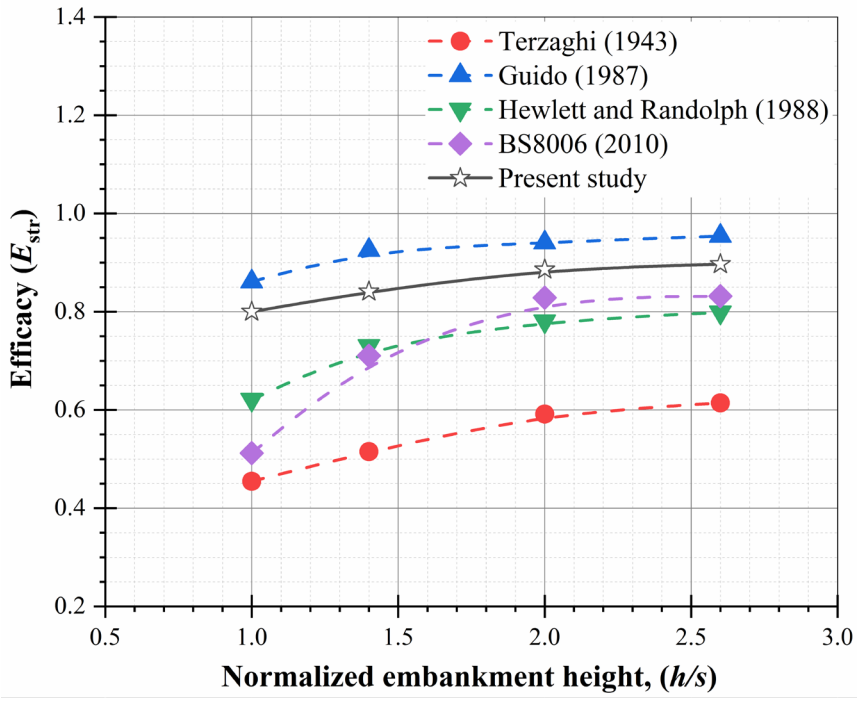

805

806 **(b)**

807 **Figure 15:** Comparison of Present study with different design methods, (a) soil arching

808 ratio (*SAR*), and (b) efficacy (E_{str})

809